Pergamon

Journal of Structural Geology, Vol. 19, Nos 3–4, pp. 481 to 502, 1997

0191-8141/97 $17.00 + 0.00

PII: S0191-8141(96)00096-X

Sequential development of selected Pyrenean thrust faults

ANDREW J. MEIGS

Division of Geological and Planetary Sciences, California Institute of Technology, Pasadena, CA 91125, U.S.A.

(*Received* 13 *December* 1995; *accepted in revised form* 9 *October* 1996)

Abstract—New mapping, structural analysis and magnetostratigraphy reveal a polyphase deformational history at the leading edge of the Spanish Pyrenean foreland fold-and-thrust belt. The present structural architecture is the consequence of three discrete periods of deformation. Map relationships between four syntectonic units and major structures provide tight geometric and age constraints for each deformational period (D_1: 55 to 42 Ma; D_2: 30.1 to 28.0 Ma; D_3: 27.9 to <25.8 Ma). Most of the shortening in the area accumulated during D_2 thrusting at rates which varied from 0.7 mm y^{-1} to 2.8 mm y^{-1} along strike from northwest to southeast, respectively. Removal of D_2 and D_3 displacement on thrust faults restores folds formed during D_1. A sequential kinematic history during which an individual structure accommodates shortening by folding, tightening of the fold and subsequent truncation by thrust faulting is inferred. Sequential restoration of three serial cross-sections demonstrates that nearly every structure active during D_1 was also active during D_2. Distributed deformation characterizes the temporal and spatial pattern on all time scales, from structures active during each individual deformational period to the long-term history encompassed by the total deformation. © 1997 Elsevier Science Ltd. All rights reserved.

INTRODUCTION

Polydeformation is a concept most commonly associated with the metamorphic internides of orogenic belts. It is recognized by the successive overprinting of fabrics and structures resulting from discrete deformational events (Ramsay and Huber, 1987). A complete description of the kinematic history of a region requires establishing a set of criteria with which individual deformational pulses may be discriminated. Because the hinterland is frequently deformed under a variety of pressure and temperature conditions, each period of deformation is often characterized by a distinct suite of structures formed within the ambient P–T conditions. In contrast, the pressure and temperature regime during deformation of the orogen's margins, e.g. the foreland fold-and-thrust belt, are less variable. Even though these regions may undergo comparable polyphase deformation, isolating discrete deformational phases is often difficult.

Such differentiation is important, however, because understanding what, where, when and how the total displacement within a cross-section accumulates is critical to understanding the long-term process of fold and fault formation and the kinematic evolution of thrust belts (Geiser, 1988). In particular, the final geometry of an individual fold or fault tells little about the incremental geometry during growth (Marshak and Mitra, 1988). Yet neither long-term fault nor fold formation can be modeled successfully unless their deformational history, particularly at intermediate stages, can be completely described.

Herein are described the results of new mapping (1:12,500) of an area greater than 225 km^2 of a portion of the Spanish Pyrenean foreland fold-and-thrust belt. Within this region, folds and thrusts developed coevally with deposition of a thick sequence of syntectonic strata. The syntectonic deposits provide unequivocal evidence of a long-lived, polydeformational structural evolution and enable a high-resolution view of the sequential development of each fold and thrust in the study area.

CONCEPTUAL FRAMEWORK

Syntectonic strata are particularly useful for structural analysis (Burbank and Raynolds, 1988; Jordan *et al.*, 1988). Angular relationships below and above unconformities, contact relationships between syntectonic strata and faults, and syndepositionally deformed strata are the tools with which the chronology of deformation can be established (Fig. 1; Armstrong and Oriel, 1965; Royse *et al.*, 1975; Alonso, 1989; DeCelles *et al.*, 1991; Coogan, 1992; Suppe *et al.*, 1992; Vergés *et al.*, 1996). Stratal geometries across unconformities preserve the tilt of beds established prior to deposition above the unconformity. Consider, for example, a clockwise rotation of beds and subsequent unconformable overlap by a new deposit (Fig. 1a). If this pattern is repeated during a series of events, a complex, but completely retrodeformable series of angular relationships are preserved across the unconformities (provided subsequent internal deformation does not substantially modify angular relationships). Alternatively, superposition of clockwise and anticlockwise rotations leads to development of opposing dips in successively younger unconformity-bounded packages (Fig. 1b). Tilting may result from either folding or rotation due to displacement on a curviplanar fault or rotation caused by footwall deformation. Contact relationships between unconformity-bound packages of beds and faults provide another constraint on the space- and time-distribution of shortening (Fig. 1c). Whereas the

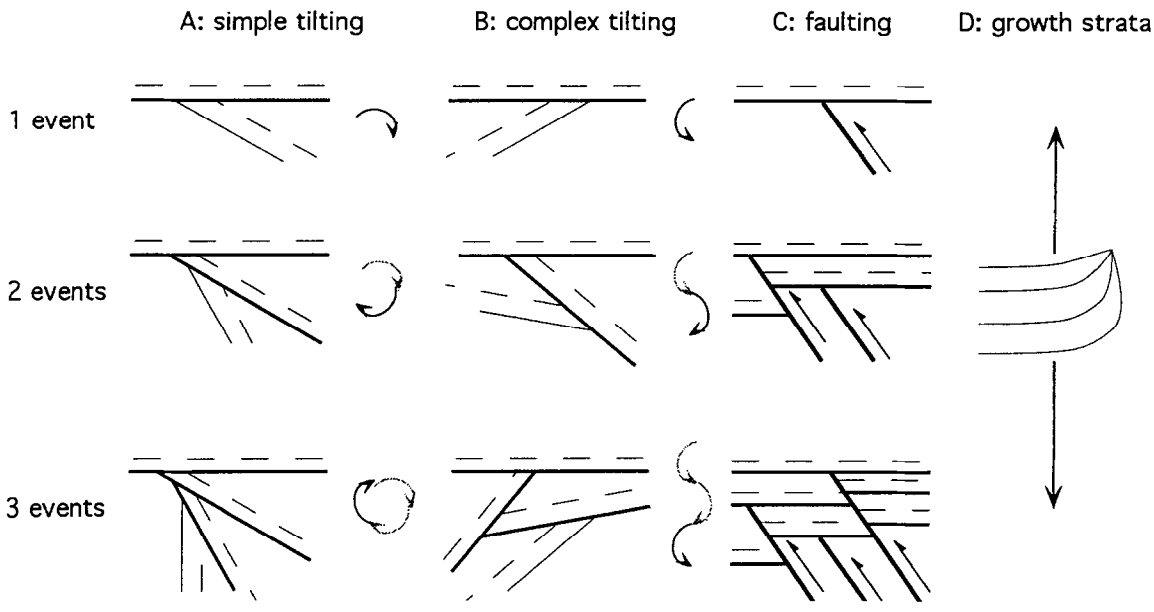

Fig. 1. Schematic diagrams illustrating interpretation deformational events from angular unconformities. (a) Simple tilting where there is a consistent sense of rotation, in a clockwise direction for this example. Note that older beds progressively steepen with time. (b) Complex tilting where clockwise and anticlockwise rotations are superimposed. Note that older beds may be rotated to shallower or steeper dips depending on the magnitude of superimposed rotations. (c) Faulting where the chronology of faults is constrained by cross-cutting relationships. Similar to paleoseismological techniques. Note that the age of faulting is bracketed by the youngest bed cut by, and the oldest bed overlying, a fault. (d) Growth strata can be difficult to use to distinguish discrete deformational pulses because their internal geometry is a function of the style of folding, sediment-accumulation rates, and variations in the rate of shortening.

tilting of beds may arise from several different mechanisms, faults that are unconformably overlain by undeformed strata describe the deformation uniquely. A third form of evidence for deformation comes from growth strata, strata deposited above actively growing structures (Fig. 1d; Riba, 1976; Anadón *et al.*, 1986; Medwedeff, 1989; DeCelles *et al.*, 1991; Suppe *et al.*, 1992; Vergés *et al.*, 1996). Each of these geometries are presented as end-members and are not mutually exclusive. In fact, many of the examples discussed later are the products of combinations of each. Although the depiction of tilting and faulting (Fig. 1a–c) imply a temporally discontinuous style of deformation whereas the growth strata imply a continuous deformation, the relative continuity of deformation is not easily determined from geometric relationships alone.

Recognizing unconformities, tilts and growth strata in well-dated syntectonic sediment allows sequential restoration of individual structures. Sequential restorations allow the incremental geometry of a cross-section in space and absolute time to be defined. Such restorations serve to define the kinematic evolution of structures precisely and give a high degree of confidence in geologic and geometric interpretations of structure (Geiser, 1988). Although overprinted structures and fabrics provide information on the relative structural sequence (Morley, 1988; Boyer, 1992), a complete description of deformation path and kinematic history depends on the availability of criteria that constrain incremental structural geometry in space and time. When these data are integrated by mapping and structural analysis, fine-scale steps in a long-lived, polyphase deformational history may be resolved with little ambiguity.

GEOLOGIC BACKGROUND AND DESCRIPTION OF STUDY AREA

Tilting, growth strata and overlapping unconformities within syntectonic strata provide excellent constraints on the temporal and geometrical evolution of foreland fold-and-thrust belts (Armstrong and Oriel, 1965; Burbank and Raynolds, 1988; Jordan *et al.*, 1988; Coogan, 1992; Muñoz, 1992; DeCelles *et al.*, 1993; Vergés, 1993; DeCelles, 1994). The south-central sector of the Spanish Pyrenean foreland fold-and-thrust belt comprises three thrust sheets carrying marine and non-marine sedimentary rocks. From north to south and in order of age of initial emplacement, they are the Bóixols, Montsec and Sierras Marginales thrust sheets (Fig. 2; Muñoz, 1992). The Sierras Marginales thrust sheet, in contrast to the other two thrust sheets, is extensively internally deformed. A complex assemblage of folds, minor thrust sheets and syntectonic strata on the northern edge of the Ebro Foreland basin (inset, Fig. 2) developed in association with the thrust sheet. A detailed record of the spatial, geometrical and temporal evolution of a portion of a foreland fold-and-thrust belt is contained within this assemblage.

The study area is located in northeastern Spain along the Aragon–Catalunya border to the northwest of Balaguer and adjacent to a large reservoir on the Rio

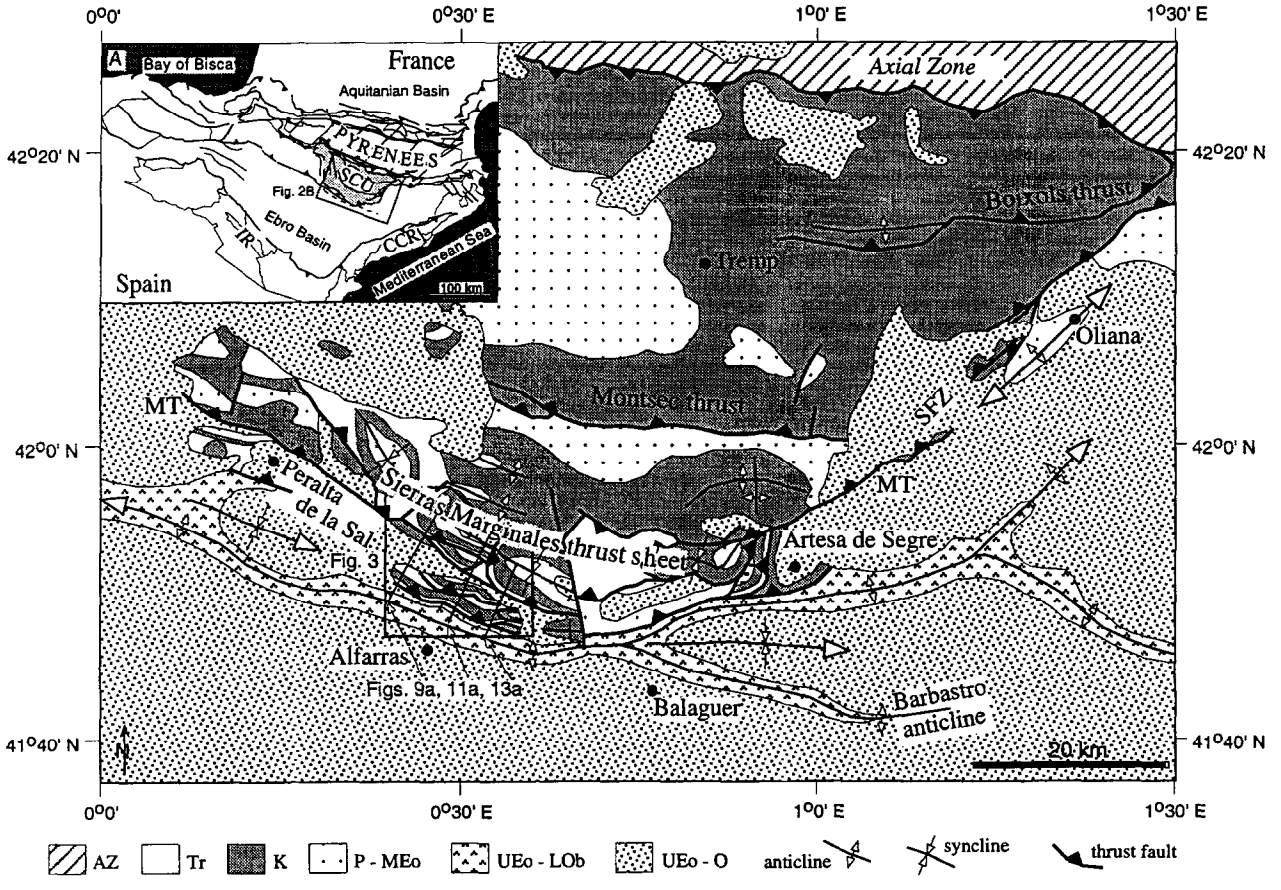

Fig. 2. (a) Regional location map. SCU = South-central unit of the Spanish Pyrenees depicted in (b). IR = Iberian Ranges, CCR = Catalan Coastal Ranges. (b) Tectonic map of the south-central unit (after Teixell, 1992). Note that the Sierras Marginales thrust fault is discontinuously exposed and defines the southern edge of the south-central unit. SFZ = Segre fault zone which is an oblique ramp system linking the eastern with the south-central Pyrenees. MT = Montargull thrust. Units are: AZ = crystalline rocks of the axial zone undifferentiated, Tr = Triassic evaporites and carbonates, K = Cretaceous rocks undivided, P–MEo = Paleocene through Middle Eocene rocks undivided, UEo–LOb = Barbastro Formation, UEo–O = Upper Eocene to Oligocene non-marine strata undivided.

Ribagorzana, the Embalse de Santa Ana (Figs 2 & 3). In a pioneering study, Pocoví (1978) delineated the basic structural and stratigraphic framework of the Sierras Marginales thrust sheet by mapping two neighboring 1:50,000 topographic sheets. His dissertation served as a key reference and foundation for this work. As a consequence of remapping this area in far greater detail, three new syntectonic units were recognized, a new interpretation of the structure and its evolution was revealed and absolute ages of both the new units and the deformation using a new magnetostratigraphic section was established.

STRATIGRAPHY

Stratigraphic units in the study area are most easily understood when considered as part of either the pretectonic or syntectonic assemblage (Fig. 3). Marine and non-marine rocks occur in each assemblage. The character of the Triassic through Paleocene pretectonic stratigraphic succession is highly variable (Pocoví, 1978). Practically every minor thrust sheet within the Sierras Marginales thrust sheet has a unique stratigraphic succession due to rapid vertical and lateral variations in both lithology and thickness. There is an overall thinning of the pretectonic section from greater than 800 m on the northern, hinterland side of the study area to less than 300 m in the southernmost thrust sheets on the foreland side. This stratigraphic variability is most likely the consequence of superposition of transgressive–regressive cycles during marine sedimentation (Pocoví, 1978) and the extreme craton-ward position of the study area with respect to the north-facing Mesozoic passive margin. Stratigraphic variability is most pronounced in the southernmost part of study area and this variability probably influenced both the style of deformation and structural complexity.

Syntectonic sediments are represented by Lower Eocene marine and Upper Eocene and younger non-marine strata (Pocoví, 1978). Four distinct unconformity-bound packages of syntectonic strata are recognized in the study area and were differentiated by angular and contact relationships, and lithologic and facies

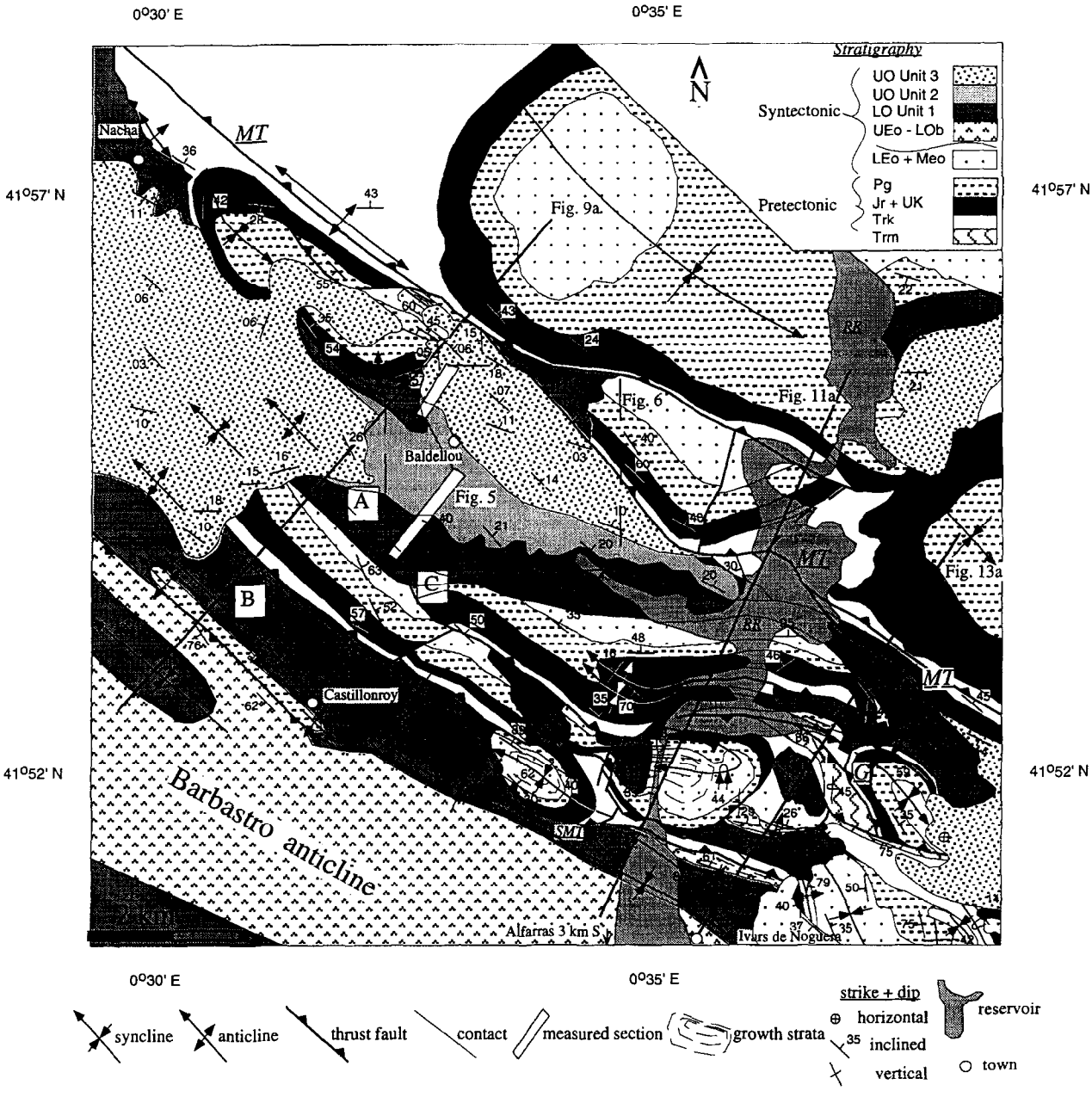

Fig. 3. Geologic map of the study area. Distribution of pre-tectonic units modified from Pocoví (1978). A, B, and C are specific areas referred to in the text. MT = Montargull thrust. RR = Rio Ribagorzana. G = Gastapá thrust sheet. Stratigraphic units are subdivided into pre-tectonic and syntectonic groups. Pre-tectonic units are: Trm = Triassic, Muschelkalk facies, Trk = Triassic, Keuper facies, Jr + UK = Jurassic and Upper Cretaceous carbonates undifferentiated, Pg = Paleocene Garumnian facies. Syntectonic units are: LEo + MEo = Lower and Middle Eocene limestones undifferentiated, UEo–LOb = Barbastro Formation, LO Unit 1 = unit 1 in non-marine strata, UO Unit 2 = unit 2, UO Unit 3 = unit 3. Break between LEo + MEo and UEo–LOb marks the change from marine to non-marine deposition in the syntectonic succession. Open box indicates location of measured section shown in Fig. 5. Box marked by dashed line shows the region of sample location map, Fig. 6. Cross-sections depicted in Figs 9, 11 and 13 are indicated by straight black lines.

variations between each package (Figs 3 & 4). Although the youngest non-marine rocks were considered previously to be post-tectonic (Pocoví, 1978), new mapping demonstrates that the non-marine succession consists of three syntectonic units. These units are described below.

Unit 1

Unit 1 crops out on the flanks of narrow synclines, interpreted to be piggyback basins formed above thrust imbrications of pre-tectonic strata (Fig. 3). Unit 1 unconformably overlies various pre-tectonic units, as

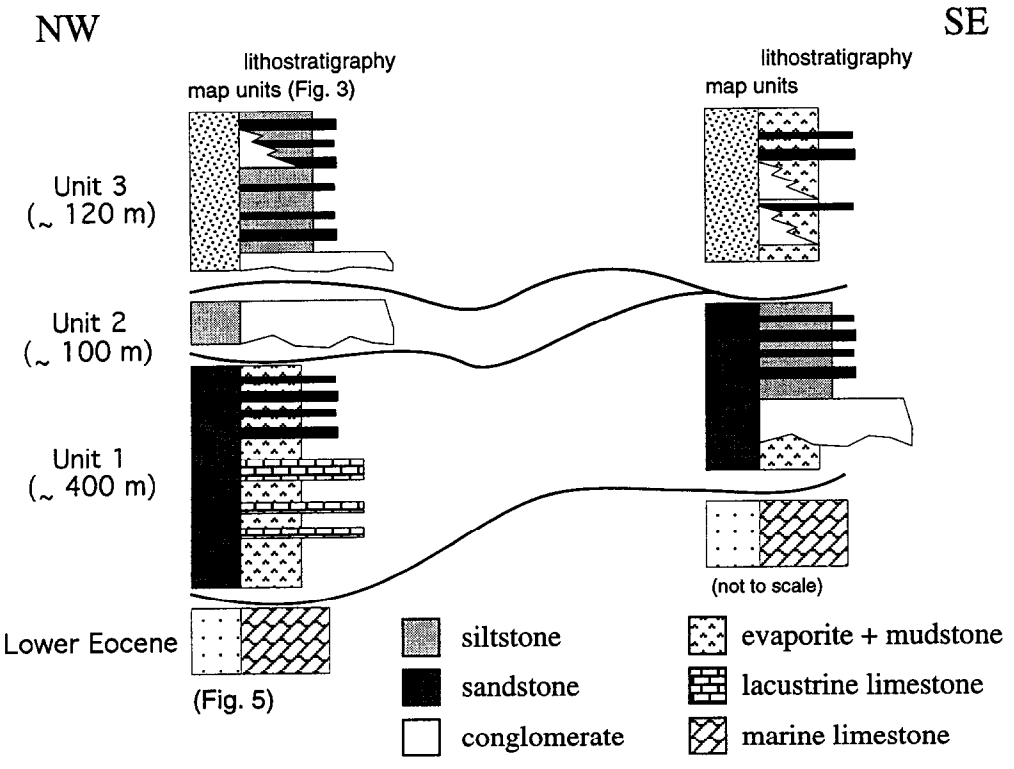

Fig. 4. Schematic stratigraphic columns depicting changes in thickness and facies from northwest to southeast along strike in the study area. Northwestern column represented by a measured section in Fig. 5. Map units are the same as in Fig. 3. Not to scale.

well as Lower and Middle Eocene syntectonic limestones. It is unconformably overlain by both units 2 and 3. The most complete exposure of unit 1 occurs in the Baldellou basin, where its thickness varies from ~400 m in the northwest to less than 200 m in the southeast (Figs 3 & 4). Sequentially younger beds onlap the unconformity at the base towards the east (A, Fig. 3). Deposition against pre-existing relief is suggested by this observation and accounts in part for lateral variations in thickness. Other factors which account for thickness variations are truncation below subsequently developed unconformities and thrust faults.

A systematic lithological variation is seen in unit 1 in the Baldellou basin. On the northwest, the section is dominated by purple–red–brown evaporites and mudstone. The lower portion of the section includes abundant, pale green, bioturbated lacustrine limestone beds, whereas the upper portion is characterized by numerous brown, climbing-ripple-laminated sandstone beds (Fig. 4). Along strike to the southeast, in contrast, the section is thinner; evaporite and mudstones are present only near the base. Otherwise, the section is dominated by orange–red siltstone and climbing-ripple-laminated sandstone beds and includes gray–orange conglomeratic beds whose clasts consist of Mesozoic, Paleocene and Lower Eocene limestones. Overall, unit 1 is interpreted to represent lacustrine deposition interfingering with fluvial and alluvial rocks locally.

Unit 2

Unit 2 is only distinguishable from units 1 and 3 on the southern and northwestern flanks of the Baldellou basin (Fig. 3). Its contact with unit 1 is an angular unconformity, but it is largely conformable with unit 3 and the contact is inferred to be a disconformity. Locally, unit 2 thins and is slightly folded where it directly overlies folds in the pre-tectonic succession. As a distinct unconformity-bounded package, unit 2 is not identifiable in southeastern parts of the study area (Figs 3 & 4).

A distinct orange–gray conglomerate with clasts from Mesozoic, Paleocene and Lower and Middle Eocene units characterizes the basal part of unit 2. Up-section, unit 2 grades into a brown–orange sequence of sandstone and siltstone. Conglomeratic lags in the bottoms of some scours contain a range of metamorphic and plutonic lithologies that indicate a hinterland provenance in the Pyrenean axial zone (Fig. 2). The sandstone–siltstone portion of unit 2 is indistinguishable from similar facies in unit 3. Unit 2 is interpreted to represent locally-sourced alluvial aprons shed-off local structural highs

into a fluvial system draining the crystalline core of the Pyrenean orogen.

Unit 3

Unit 3 forms a relatively thin blanket of sediment which is widely exposed in the northwestern and southeastern portions of the study area (Fig. 3). Most of the structures in the area, in addition to units 1 and 2, are unconformably overlain by unit 3. Unit 3 is truncated by the Montargull thrust.

Like unit 1, unit 3 shows marked lithologic variation along strike. In the northwest, unit 3 is dominated by brown siltstone and channelized sandstone (Fig. 4). Conglomeratic lags within many channels consist of metamorphic and plutonic clasts of axial zone origin. Pre- and syntectonic gray–orange conglomerate-clast beds interfinger with the sandstone–siltstone intervals. Along strike to the southeast, unit 3 is dominated by white–gray evaporites and mudstone that interfinger with gray–orange conglomerates and occasional sandstones (Fig. 4). Paleocurrent indicators from within the conglomerates indicate paleoflow at a high angle to local structural trends. Unit 3 is interpreted to represent largely fluvial deposition from rivers draining the axial core of the Pyrenees. Interfingering between locally-sourced alluvial aprons and adjacent lacustrine and fluviatile lithologies suggests local structural highs shed detritus into adjacent structural lows.

AGES OF SYNTECTONIC UNITS

Lower and Middle Eocene limestone ages are constrained biostratigraphically (Pocoví, 1978). A paleomagnetic section was collected across the Baldellou basin (Baldellou section) to constrain the ages of units 1–3. A nearly continuous lithostratigraphic section, ~610 m long, was measured (Fig. 5). More than 220 paleomagnetic samples were collected at 57 sample sites spaced at ~10 m intervals across the section (Fig. 6). Typical sample lithologies included mudstone, siltstone and rarely, fine grained sandstone. The resultant magnetic stratigraphy is believed to represent a relatively complete record. In order to minimize the amount of time missing across the unconformities separating units 1, 2, 3, the section was sampled at places where there was minimal angular discordance between units (Fig. 6).

Details of paleomagnetic analysis

Thermal demagnetization is the most reliable technique for establishing the characteristic remanence in weakly magnetized Spanish red-beds (King-Powers, 1989; Burbank *et al.*, 1992a, b; Meigs *et al.*, 1996). A step-wise thermal demagnetization pilot study was conducted on pairs of samples chosen to cover the range of sample color and lithology. The samples of the pilot study were demagnetized at 50°C temperature steps up to 550°C, 30°C temperature steps to 640°C and then at one final step to 710°C (Fig. 7a). The characteristic remanence is interpreted to have been disclosed between 250 and 350°C, given that directions remained stable and that intensity decreases were relatively small above this temperature. The increase in intensity above 500°C probably reflects the authigenic growth of new minerals as a consequence of the thermal demagnetization process. Consequently, the remaining samples were demagnetized at 250, 300 and 350°C temperature steps. Hematite, with components likely contributed from both the cements and detrital grains, is interpreted to be the primary carrier of the remanence because rock color is dominated by red, purple, orange and brown.

After blanket thermal demagnetization of the entire suite of samples, paleolatitudes were determined from the virtual geomagnetic poles (VGP) at each site. These VGPs served as the basis for assignment of normal or reversed polarity for each site (Fig. 5). Data quality was quantified for the groups of samples at each site by calculation of the Fisher (1953) precision parameter, k. For each temperature level at a given site, samples were classified as 'class I' for Fisher $k \geq 10$, 'class II' for $k < 10$ but the magnetic direction is unambiguous and 'class III' when the sample directions were too dispersed. Normal or reversed polarity was assigned to a given site using the VGP of the temperature step with the highest k value at that site.

Paleomagnetic results

The data are of good quality: 55% of the sites are class I, 40% are class II and 5% are indeterminate (3 sites). A magnetopolarity stratigraphy consisting of 12 magnetozones was created based on these data (Fig. 5). With exception of three single-point magnetozones (N2, 3 and 5), all the magnetozones contain at least one class I site. Single site reversals whose error bar overlapped 0° latitude were disregarded. The data pass the reversal test, but they fail the fold test at the 95% confidence level (Fig. 7b and Table 1). It is not surprising the data fail the fold test because the section was collected through a single moderately north-dipping panel of strata characterized by moderate to low dips (Fig. 6).

Correlation of the Baldellou section with the geomagnetic polarity time scale, like many paleomagnetic sections developed in non-marine strata, is problematic. Stratigraphic correlation of units 1–3 with comparable units at Peralta de la Sal (Senz and Zamorano, 1992) and depositional, lithostratigraphic and structural similarities between the study area and Artesa de Segre 40 km to the east (Meigs *et al.*, 1996) provide reasonably tight constraints on the possible age of the section, despite the fact that biostratigraphic data for the region are scarce. Map and stratigraphic relationships indicate that unit 1 and unit 3 are likely temporal correlatives of the Peraltilla and Sariñena Formations at Peralta de la Sal, respec-

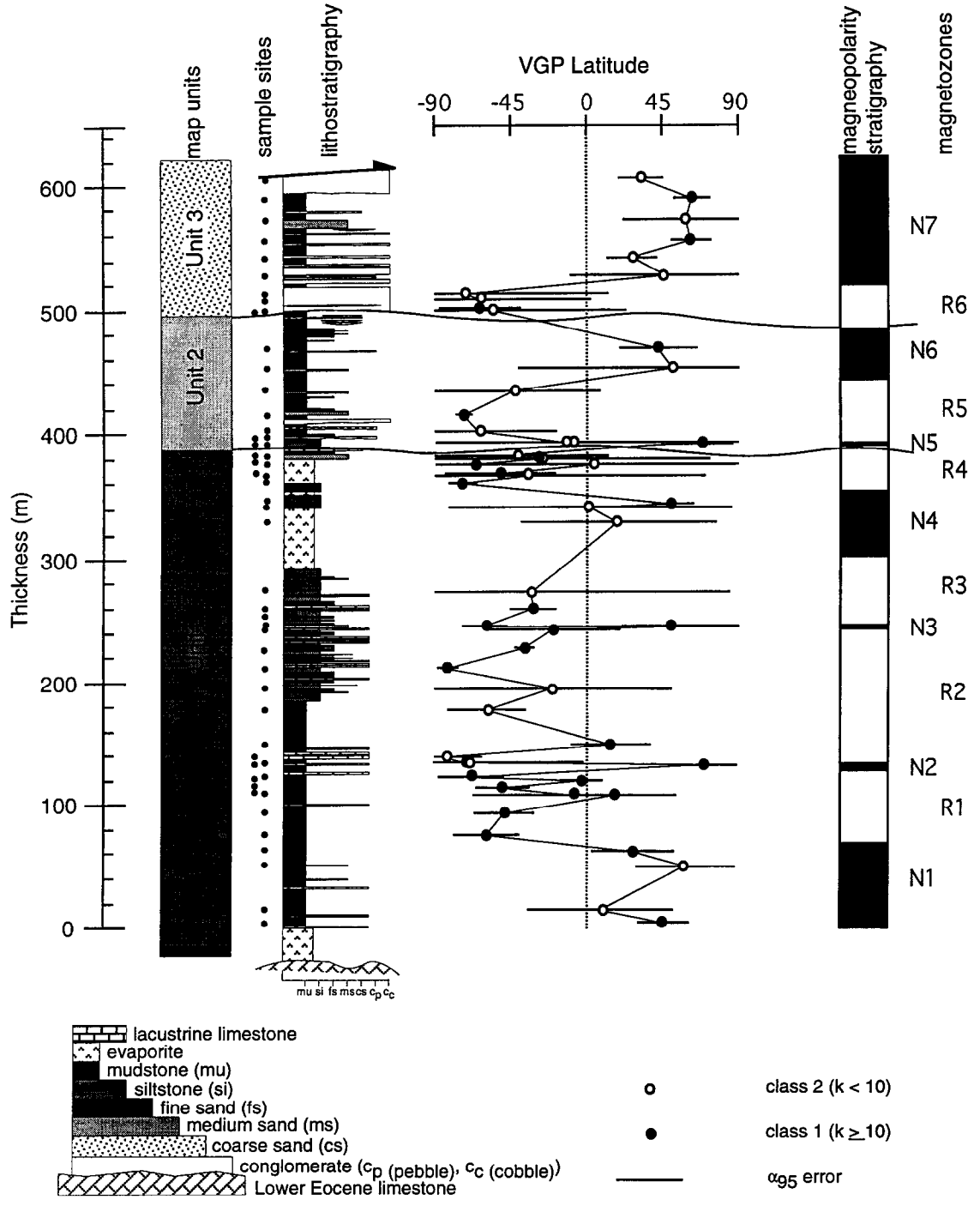

Fig. 5. Measured section, latitudes determined from virtual geomagnetic poles (VGP) of sample sites, and magnetopolarity stratigraphy for Baldellou piggyback basin fill. Note that the section begins above the unconformity at the base where the section overlies Lower Eocene limestones. Class I is based on Fisher (1953) precision parameter ($k \geq 10$) and class II is $k < 10$. *N1* denotes normal magnetozone 1, *R1* denotes reversed magnetozone 1. Boundaries between magnetozones were arbitrarily drawn halfway between sites of opposite polarity. See Fig. 3 for location.

tively. The Peraltilla and Sariñena Formations are thought to be upper Lower Oligocene (Upper Rupelian (?)) and Upper Oligocene (Upper Chattian (?)), respectively, based on extrapolation of biostratigraphically determined ages in similar rocks exposed elsewhere in the Spanish Pyrenean Foreland (Crusafont *et al.*, 1966; Sudre *et al.*, 1992; Senz and Zamorano, 1992). At Artesa de Segre, the depositional and structural history of two non-marine units bear a striking similarity to those of units 1 and 3. A deformed lacustrine unit deposited directly on top of previously deformed pre-tectonic strata in the hanging-wall of the Sierras Marginales thrust sheet is dated paleomagnetically as ~29.5–28.5 my old (Early (Rupelian)–Late Oligocene (Chattian) boundary, Meigs

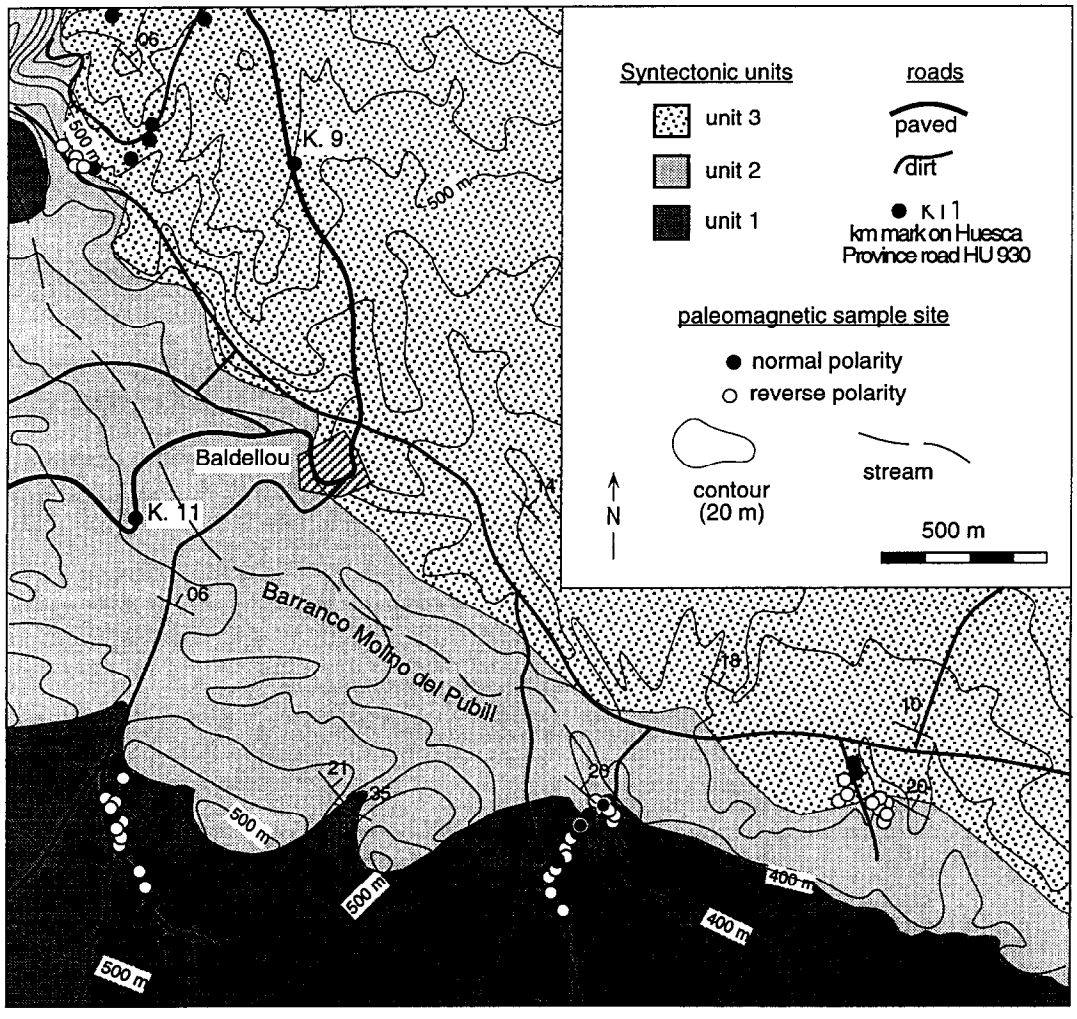

Fig. 6. Sample location map. Sample sites are indicated by dots, black if the site mean polarity indicates normal polarity, white if reversed polarity.

Table 1. Fisher statistics, fold and reversal tests on paleomagnetic data

Data Set	N	k	$\alpha 95(°)$	Declination (°)	Inclination (°)
Normal polarity samples					
In situ	34	7.9	9.3	59.4	14.0
Bedding-corrected	34	8.1	9.2	18.4	35.2
Reverse polarity samples					
In situ	56	7.6	7.4	178.5	−77.7
Bedding-corrected	56	9.5	6.5	200.0	−47.4

Fold test (Butler, 1992): pass if k, bedding-corrected/ k, *in situ* $> F(n$, bed; n, *in situ*; 0.05)
Normal polarity: = 8.1/7.9 = 1.03 < 1.84 Reverse polarity: = 9.5/7.6 = 1.25 < 1.53

Reversal test (McFadden and McElhinny, 1990):
pass if k, bedding-corrected/ k, bedding-corrected, normal $< F(n$, rev; n, norm; 0.05)
= 9.5/8.1 = 1.17 < 1.74

Note: k = best estimate of the Fisher (1953) precision parameter. α_{95} = 95% confidence interval on mean.

Bedding corrected data restored to horizontal attitude assuming non-plunging, cylindrical folds.

Fold test using precision parameters for mean directions of bedding-corrected and *in situ* data as described in Butler (1992) is a statistical F test. Value for F (N, bedding-corrected, N, *in situ*, confidence level (95%)) taken from table of F values from a standard statistics textbook.

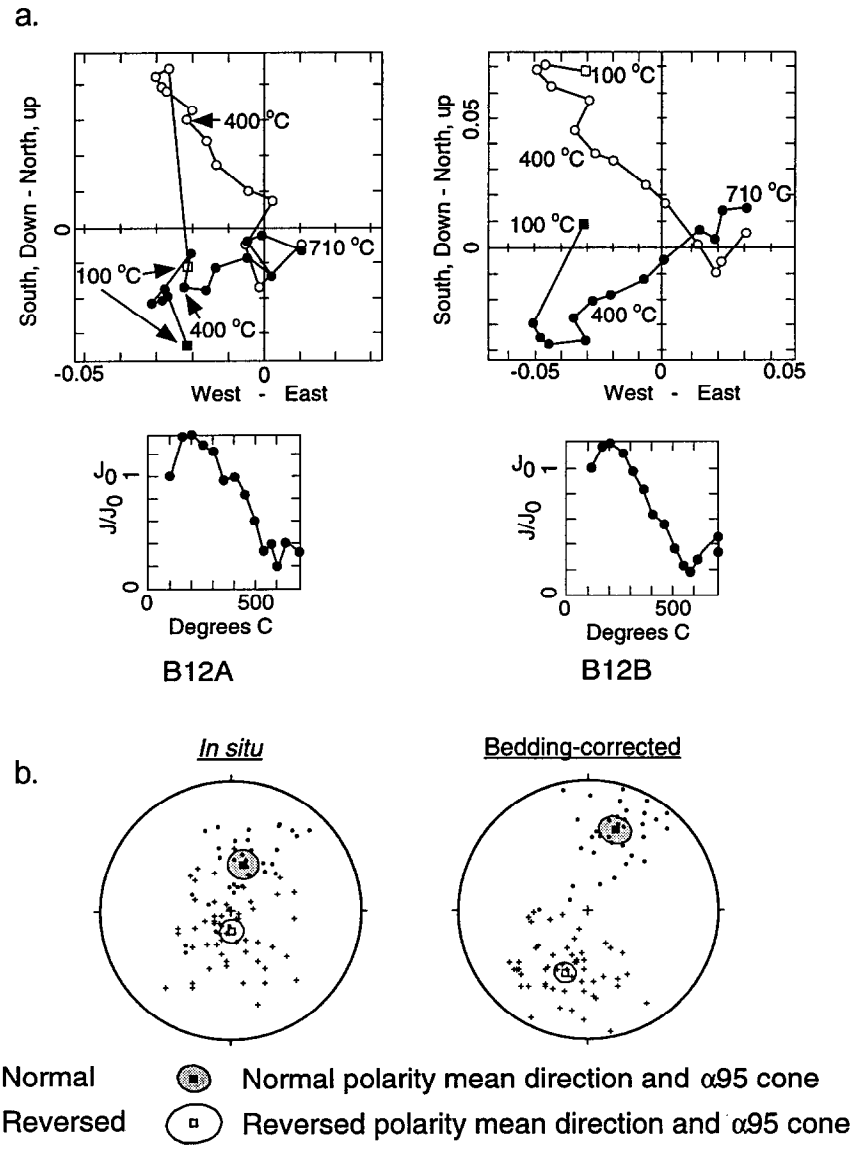

Fig. 7. (a) Zijderveld plots of inclination (open circles) and declination (filled circles) data from representative samples in the section and plots of intensity (J) versus temperature. The site mean direction indicates reversed polarity for sample B12 (southwest declination, up inclination). (b) Stereonet plots of *in situ* and bed corrected class I data with 95% confidence interval on mean direction (α_{95}). Note that section passes the reversal test and there is no apparent rotation in the section.

et al., 1996). Stratigraphically overlying this unit is a succession of brown fluvial strata whose source is the core of the Pyrenees. This unit is cut by the Montargull thrust, but is otherwise little deformed and unconformably overlies all previously formed structure. Its age ranges from 27.8 to less than 24.9 Ma. Although it is not possible to correlate physically the strata at Artesa with units 1 and 3, the close similarities in both depositional and structural histories are suggestive of the possible age of the Baldellou section. Given these similarities, an Oligocene age for the section is suggested.

Two potential correlations are presented and differ only in the correlation of unit 1 (Fig. 8a & b). The 'older' correlation implies a steady sediment accumulation rate of 0.08 mm y^{-1} (Fig. 8a & c), one criteria used to evaluate a correlation with the geomagnetic polarity time scale (Talling and Burbank, 1993). The younger correlation is preferred, however, for the following reasons. (1) Ages of upper Lower Oligocene through middle Upper Oligocene for units 1–3 are consistent with the approximate ages of correlative units at Peralta de la Sal (Senz and Zamorano, 1992). (2) The age range of units 1–3 and the implications for structure are consistent with the age of units and structural chronology at Artesa de Segre (Meigs *et al.*, 1996). (3) Given the 25.6 Ma age of the top of unit 3, the age of latest displacement on the Montargull thrust is consistent with the age of the thrust at Artesa de Segre (Meigs *et al.*, 1996) and Peralta de la Sal (Senz and Zamorano, 1992). (4) Lithofacies and sediment-accumulation rates of rocks deposited in small piggyback basins formed on top of the Sierras Marginales thrust sheet at Artesa de Segre are strikingly similar to those in the study area. (5) Unit 1 would be younger, rather than age equivalent, with the Barbastro evaporite whose age is

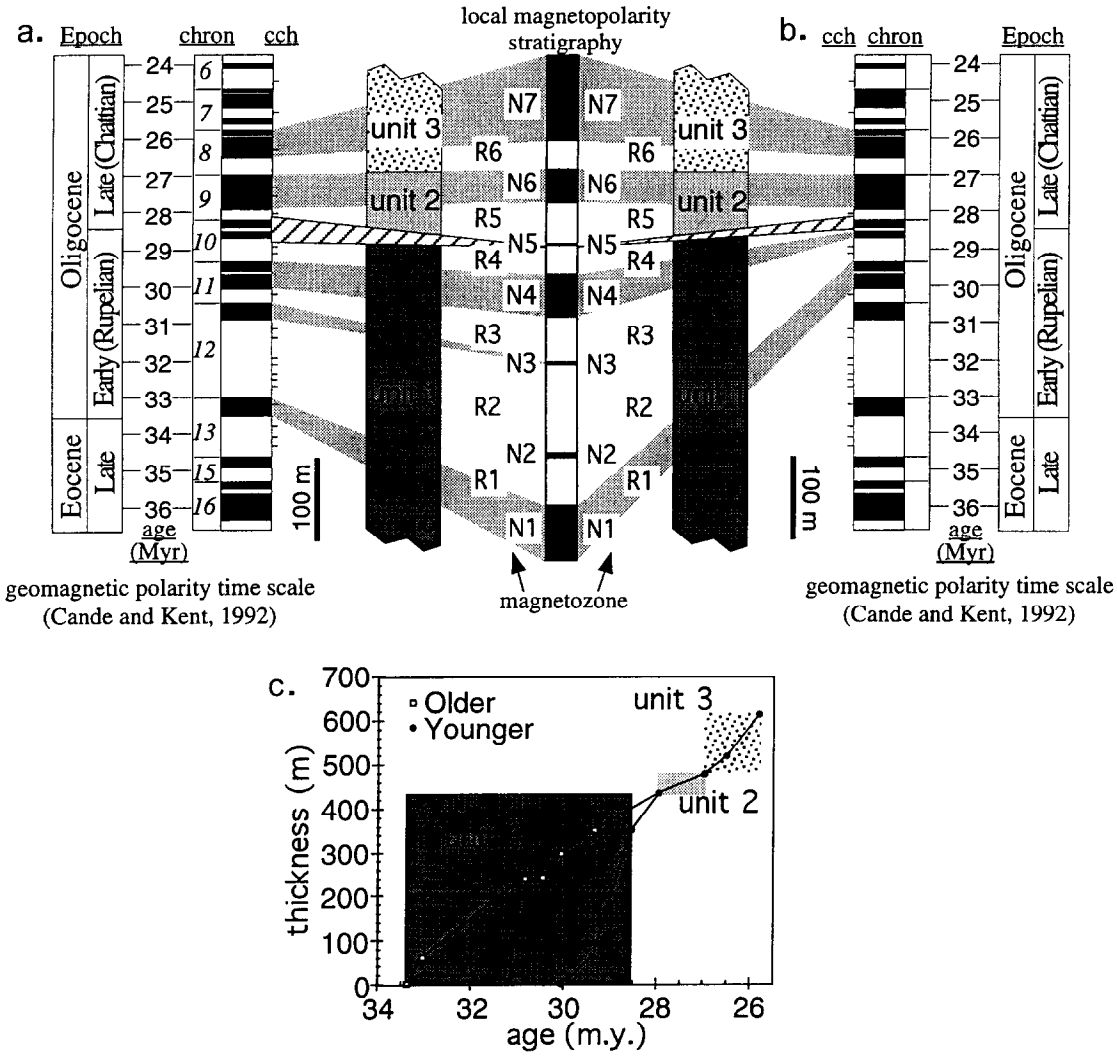

Fig. 8. Alternative correlations of magnetopolarity stratigraphy with the geomagnetic polarity time scale of Cande and Kent (1992). The approximate top of the Barbastro Formation is indicated (Colldeforns, pers. com.). (a) 'Older' correlation where unit 1 represents all the Early Oligocene. (b) 'Younger' correlation where unit 1 is Lower to lower Upper Oligocene in age. Units 2 and 3 correlate to the same part of the global time scale in both interpretations. Note that only the contact between units 1 and 2 is inferred to have appreciable time missing. Cryptochrons (cch) are denoted by short dashes next to chrons. (c) Sediment accumulation curves constructed by plotting the age of a magnetozone boundary versus its height for the older and younger correlations. Note that the older correlation yields a slow, steady sediment-accumulation rate whereas the younger sediment-accumulation curve is marked by initially high then slower rates with time.

inferred to be Lower Oligocene just to the south of the study area (Colldeforns, pers. comm.). Unit 1 was therefore deposited between 30.1 and 28.5 Ma, unit 2 between 28.0 and 27.0 Ma and unit 3 between 27.0 and < 25.8 Ma (Fig. 8b).

DEFORMATIONAL AGES AND SEQUENTIAL RESTORATION STRATEGY

The structural style and extent of deformation is complex and variable along strike (Figs 3, 9a, 11a & 13a). To describe completely the structural geometries, along-strike complications and variations in style and the evidence for the kinematic evolution, three cross-sections have been drawn from northwest to southeast. From northwest to southeast and in order of increasing complexity and shortening the sections are: Baldellou, Ribagorzana and Ivars (each section is named for the nearest local village or obvious geographic marker; Fig. 3). Key structures and stratigraphic evidence in the form of tilt/unconformity, fault/unconformity, or growth strata relationships (Fig. 1) are detailed along each section and clearly document three distinct periods of deformation (D_{1-3}).

D_1 structures are reflected by angular unconformities below unit 1 or growth strata in Lower or Middle Eocene limestones. The limestones are Ilerdian–Lutetian (55–42 Ma) in age (Pocoví, 1978), based on lithologic and faunal similarity with Ilerdian–Lutetian deposits preserved to the north of the study area (Mutti *et al.*, 1985). The age is imprecise due to extrapolation of biostratigraphically determined ages into the study area. Consequently, the duration of D_1 represents a conservative

maximum estimate of the deformational pulse. Tilting, folding and faulting of unit 1 indicate D_2 deformation. D_2 affects unit 1 and older strata but not units 2 and 3 and is bracketed by the age of the base of unit 1 (30.1 Ma) and the base of unit 2 (28.0 Ma). Structures that deform units 2 and 3 represent D_3 deformation. The duration is bracketed by the base of unit 2 (28.0 Ma) and the top of the section (<25.8 Ma). Because the top of the section is cut by a thrust, the upper age limit on D_3 represents a minimum age: D_3 may have been continued after 25.8 Ma.

The depth (~ sea level, 0 m) and dip (2–3°) of the detachment at the base of the Sierras Marginales thrust sheet in Triassic evaporites is constrained by measured sections in the pre-tectonic strata (Pocoví, 1978) and the projection of surface dip data to depth. Structures formed above a second regionally significant detachment, localized near the base of the foreland-basin succession and not seen on the sections, are not considered in detail here (Pocoví, 1978; Martínez-Peña and Pocoví, 1988; Muñoz, 1992; Senz and Zamorano, 1992). Each section is bounded on the southwest by the northeast limb of the Barbastro anticline (Fig. 3). On the northeast, each section is bounded by the Montargull thrust and one of two regionally developed hanging-wall synclines. One final note, there are a few unusual structural geometries within the cross-sections associated with notably large map occurrences of Triassic evaporites and are inferred to be related to late-stage diapirism that obscures some geometric relationships (Fig. 3).

Discussion of each section, Baldellou, Ribagorzana and Ivars, consists of (1) a description of field evidence for D_{1-3} (Figs 10, 12 & 14) and (2) a set of four cross-sections that illustrate the residual geometry for each structure after the effects of D_3, D_2 and D_1 are sequentially restored (Figs 9, 11 & 13). Jurassic through Paleocene pre-tectonic strata are line-length balanced and the Triassic evaporites are area-balanced in each step. Total thrust displacement is recovered for thrusts whose hanging-wall cutoff is preserved. Minimum displacement is recovered for thrusts with eroded hanging-wall cutoffs by restoring the hanging-wall to the base of the associated footwall ramp. Sequential reconstruction of each section involved backstripping successive structural overprints resulting from each deformational episode. Tilted rocks were restored to their inferred pre-deformational depositional geometry (DeCelles *et al.*, 1991; Vergés *et al.*, 1996). Because nearly all the unconformities are angular unconformities, residual tilt in rocks below unfolded beds is a reflection of the

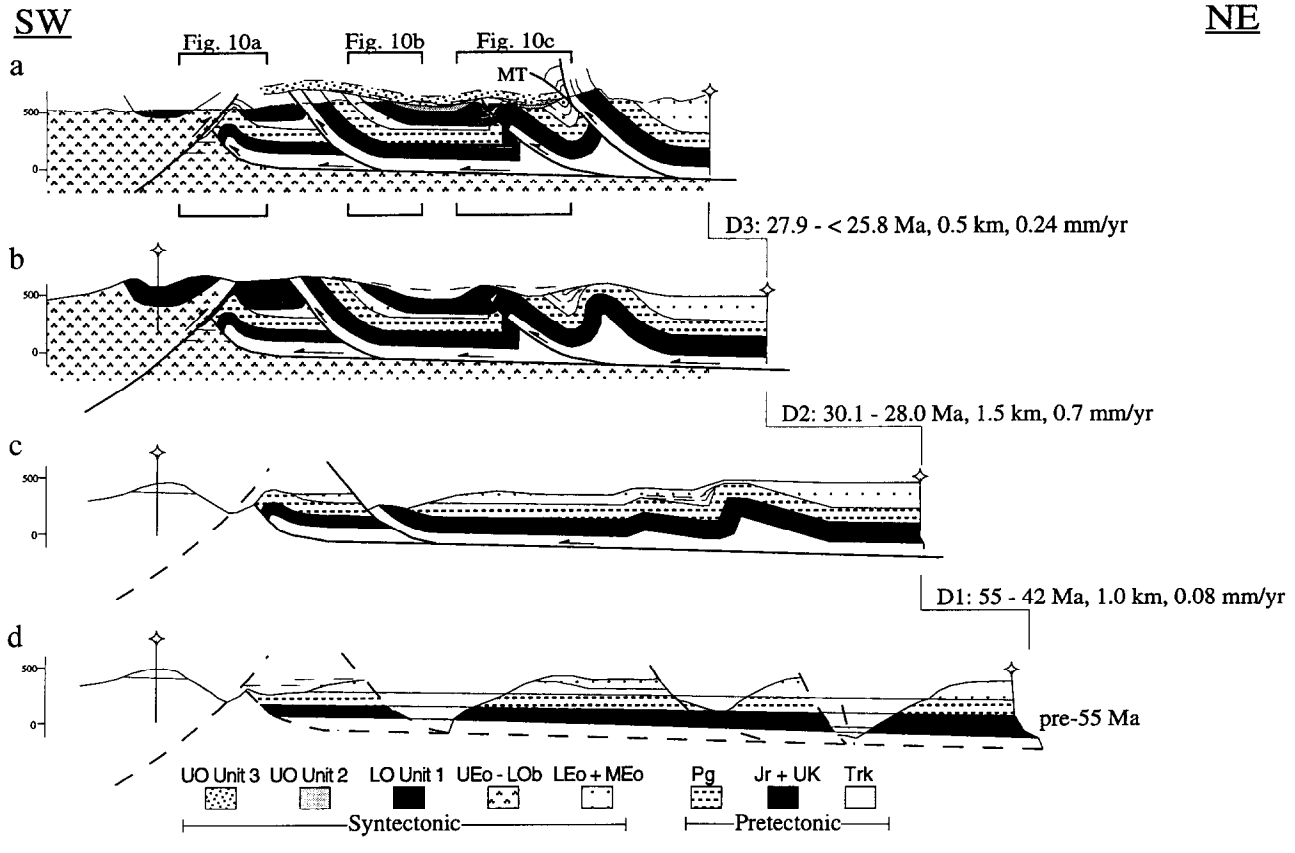

Fig. 9. Sequential restoration for the Baldellou section. Each deformational pulse, 1 through 3, is denoted by D_1, D_2, or D_3 and is followed by the age range, amount of shortening in kilometers (km), and shortening rate in millimeters per year (mm yr^{-1} = km my^{-1}). (a) Present, post-D_3 cross-section. (b) Pre-D_3, post-D_2 cross-section. (c) Pre-D_2, post-D_1 cross-section. (d) Fully restored, pre-D_1 cross-section. Age span of D_1 given by biostratigraphic data (Pocoví, 1978). Units are the same as Fig. 3. MT is the Montargull thrust. The positions of the detailed sections in Fig. 11 are indicated by open boxes. See Fig. 3 for location.

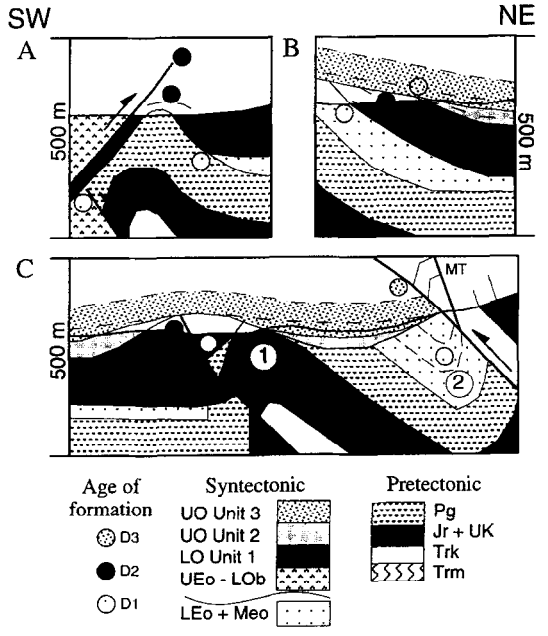

Fig. 10. Details of the Baldellou section. D_1, D_2, and D_3 refer to structures and tilts formed during deformational pulses 1, 2, and 3, respectively. Stratigraphic and/or structural evidence for a particular deformational pulse are denoted by shaded dots. MT is the Montargull thrust. Units as in Fig. 3. Circled numbers are points on sections referred to specifically in the text.

pre-depositional geometries of folds, thrust faults and thrust sheets (Fig. 1). Each section (Figs 9, 11 & 13) represents restoration of internal structures with respect to the leading edge of the Sierras Marginales thrust sheet and does not include restoration of the Sierras Marginales thrust sheet to its footwall cutoff. This analysis is only concerned with intra-thrust sheet structures, not its primary translation. Folds that affect the foreland-basin succession in the immediate footwall of the thrust sheet, including the northeast limb of the Barbastro anticline, are included because they affect units 1 and 3 (Fig. 3).

STRUCTURAL GEOMETRIES, SEQUENTIAL RESTORATIONS AND IMPLICATIONS FOR THE INCREMENTAL DISPLACEMENT FIELD

Baldellou—structural geometries

Every structure along the Baldellou section preserves evidence of D_1 deformation (Fig. 9). A clear angular unconformity between the base of unit 1 and Palaeocene strata is seen on the southwesternmost structure (Fig. 10a). An angular unconformity at the base of unit 1 and

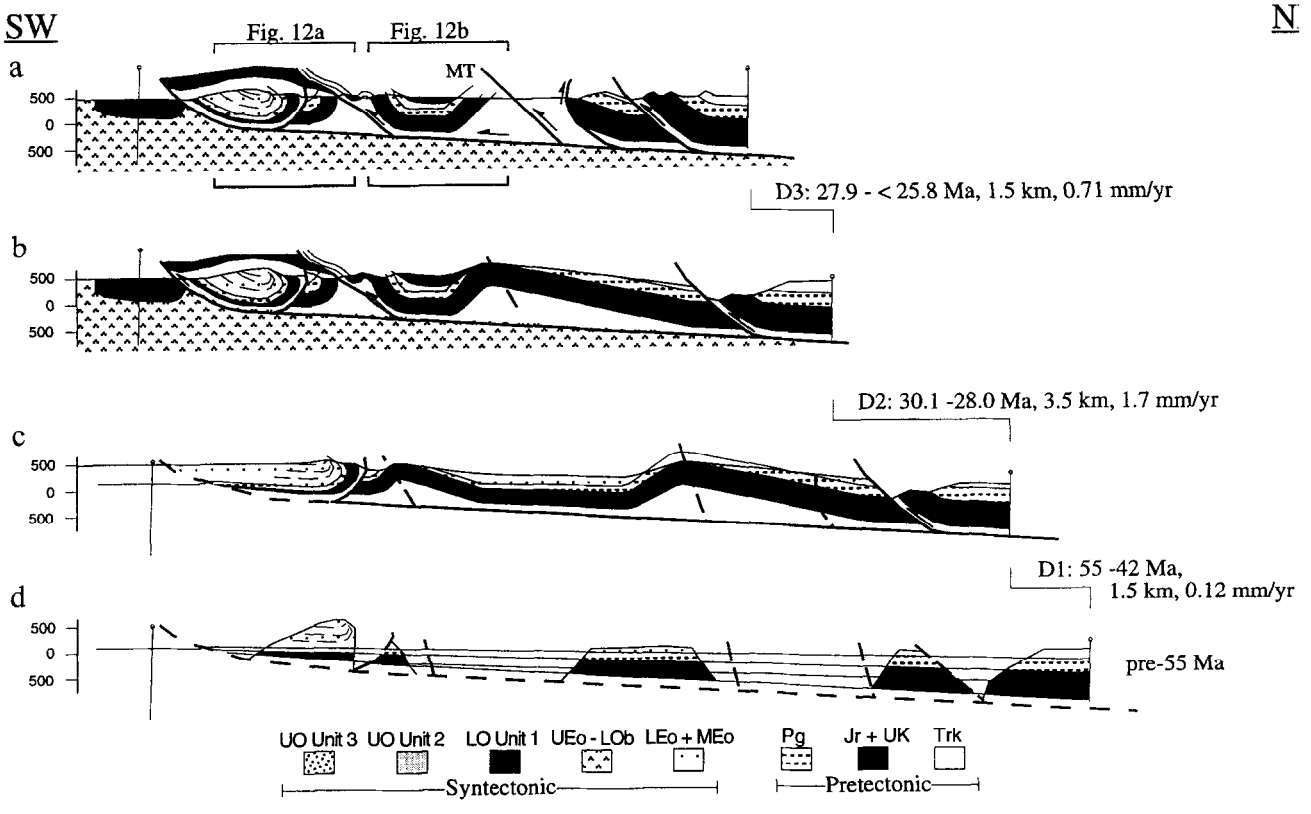

Fig. 11. Sequential restoration for the Ribagorzana section. Each deformational pulse, 1 through 3, is denoted by D_1, D_2, or D_3 and is followed by the age range, amount of shortening in kilometers (km), and shortening rate in millimeters per year (mm yr^{-1} = km my^{-1}). (a) Present, post-D_3 cross-section. (b) Pre-D_3, post-D_2 cross-section. (c) Pre-D_2, post-D_1 cross-section. (d) Fully restored, pre-D_1 cross-section. Age span of $D1$ given by biostratigraphic data (Pocoví, 1978). Units are the same as Fig. 3. MT is the Montargull thrust. The positions of the detailed sections in Fig. 13 are indicated by open boxes. See Fig. 3 for location.

onlap of unit 1 beds against that unconformity are seen on the hanging-wall of the next thrust sheet to the northeast (Figs 3 & 10b). Several different observations provide evidence of D_1 deformation on the family of structures to the northeast (Fig. 10c). Erosional removal of Lower Eocene and Paleocene rocks below an angular unconformity at the base of unit 1 can be seen on the southern anticline of an un-named anticline–syncline pair in the footwall of the Montargull thrust (1, Fig. 10c). Growth strata preserved in Lower Eocene limestones in the syncline, now cut by the Montargull thrust, document Early Eocene deformation (2, Fig. 10c). Each angular unconformity, and accompanying erosional truncation, and the growth strata are interpreted to reflect folding prior to deposition of unit 1.

Unit 1 is deformed throughout the Baldellou section and documents D_2 deformation (Figs 3 & 10). On the plunging ends of the southwesternmost structure on the section, unit 1 is folded about an anticline exposed in Paleocene strata (Figs 3 & 10a). Unit 3 clearly unconformably overlies the next thrust to the northeast and a strong angular unconformity is seen in hanging-wall strata below, including unit 1 (B, Figs 3 & 10b). To the northeast, unit 1 is folded and faulted by a well-exposed anticline and thrust (1, Fig. 10c). Although no clear growth stratal relationships can be seen in unit 1, this deformation is inferred to have occurred during and after deposition of unit 1, but prior to deposition of units 2 and 3.

Broad open folding and displacement on the Montargull thrust are the products of D_3 deformation in the vicinity of the Baldellou section (Fig. 3). Locally beds in unit 3 dip between 20 and 30° (Fig. 10b). The Montargull thrust is exposed on the northeastern end of the section and clearly truncates unit 3 (Figs 3 & 10c). Unit 2 is only identifiable as a distinct stratigraphic unit along the Baldellou section. It overlies and onlaps structures affecting unit 1, is slightly tilted and is restricted to structural lows between thrusts or in synclinal troughs (Figs 3 & 10b, c).

Baldellou—sequential restoration and incremental displacement field

The Baldellou section is characterized by the least shortening and structural complexity of the three sections. Four small-displacement south-vergent thrusts that root into the Sierras Marginales thrust and one north-vergent thrust that roots into a deeper detachment at the base of the foreland-basin succession define the structure of the present-day cross-section (Fig. 9a; Meigs *et al.*, 1992). D_3 events comprised displacement on the Montargull thrust and gentle folding of units 2 and 3 (Figs. 3 & 10b & c). Most of the 0.5 km of shortening during this phase is accounted for by displacement on the Montargull thrust. A shortening rate during D_3 of 0.24 mm y^{-1} represents a maximum, given that the Montargull thrust cuts the youngest part of the section. Reconstruction of an anticline by rejoining the hanging-wall anticline and footwall syncline of the Montargull thrust is the most profound consequence of this restoration (Fig. 9a & b). A bulk tightening of pre-existing structures in the thrust sheet, resulting in slight geometric modification of those structures, is reflected by broad folds in units 2 and 3. This folding accounts for an inconsequential amount of shortening that was not restored.

D_2 structures account for the greatest amount of shortening, 1.5 km, of any of the deformational periods on the Baldellou section. This restoration step requires removal of slip on the north-vergent thrust on the southwestern end of the section, partial unfolding of the fold at the leading edge of the thrust sheet, back rotation of faults until beds in unit 1 are subhorizontal and fold reconstruction due to removal of fault displacement on faults which cut unit 1 (Fig. 10). The anticline in the former position of the Montargull thrust is inferred to have been modified during D_2 as a consequence of translation over the lower part of a fault at depth (Fig. 10b & c). Therefore, every structure on the section was active during D_2 deformation yielding an average rate of shortening, 0.7 mm y^{-1}, twice the D_3 rate. Note that a complete restoration does not result from removal of D_2 structure. Folds decrease in amplitude and increase in wavelength and fault slip is recovered, but shortening remains in the section (Fig. 9c). In cases where a hanging-wall anticline is not preserved and a footwall syncline is not seen, it is not possible to determine uniquely whether fault restoration reconstructs a fold, like that for the Montargull thrust, or only recovers a pre-existing fault.

Every structure on the section has evidence of D_1 deformation (Fig. 9c). For the remaining folds and faults, angular unconformable relationships between unit 1 and underlying strata document D_1 deformation. 1.0 km of shortening is accounted for by these structures and accumulated over a maximum duration of 13 my at a minimum rate of 0.08 mm y^{-1}. The reconstructed stratigraphic wedge displays a gradual northward thickening of the pretectonic strata (Fig. 9d).

Ribagorzana—structural geometries

Field evidence for D_1–D_3 deformation along the Ribagorzana section only occurs in association with a suite of structures at the leading edge of the Sierras Marginales thrust sheet (Figs 3 & 11). A thick sequence of growth strata in Lower Eocene limestones is exposed on the east bank of the Rio Ribagorzana (1, Fig. 12a). A second unconformity across which pretectonic strata are tilted with respect to Middle Eocene (?) limestones (2, Fig. 12a) has been projected into section along strike from Ivars section. Both of these geometric relationships are interpreted to be the consequence of D_1 deformation. A thin veneer of unit 1(?) strata unconformably overlie the large growth sequence in the Lower Eocene lime-

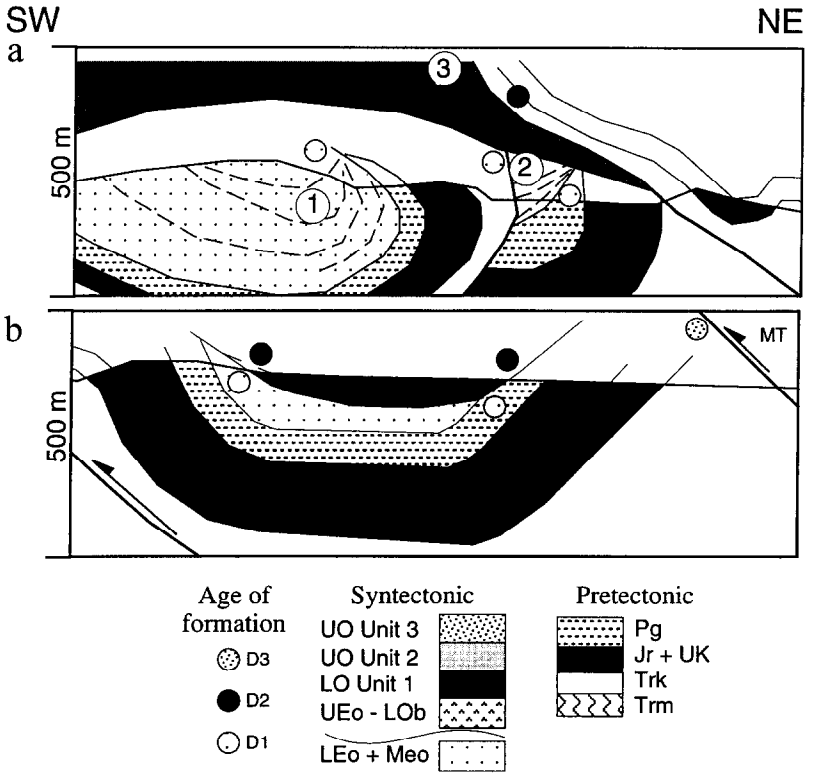

Fig. 12. Details of the Ribagorzana section. D_1, D_2, and D_3 refer to structures and tilts formed during deformational pulses 1, 2, and 3, respectively. Stratigraphic and/or structural evidence for a particular deformational pulse are denoted by shaded dots. MT is the Montargull thrust. Units as in Fig. 3. Circled numbers are points on sections referred to specifically in the text.

stones. These unit 1 strata have a growth-strata geometry in the immediate footwall of a thrust that truncates them (3, Fig. 12a). This growth sequence and the thrust truncation provide evidence for D_2 deformation. Unit 1 is schematically projected onto the Ribagorzana section to illustrate its unconformable relationship with pre-growth strata on the limbs of the next syncline to the northeast (Fig. 12b). There is no direct evidence for D_3 on this section; the Montargull thrust duplicates Triassic evaporites on the line of section and no rocks similar to unit 3 are exposed (Figs 3 & 7b).

Ribagorzana—sequential restoration and incremental displacement field

Evidence for the sequence of deformation along the Ribagorzana section comes from outcrops on the southern side of the section and by extrapolation of relationships along strike from both the Baldellou and Ivars sections (Figs 11 & 13). D_3 shortening is difficult to constrain because unit 3 does not outcrop in the section. Because both the Montargull and a related imbricate thrust cut unit 3 along strike to the northwest or southeast of the line of section (Fig. 3), they are interpreted to have the same amount of D_3 shortening as observed in neighboring sections (1.5 km, Fig. 11b). Although the shortening rate is higher, 0.71 mm y^{-1}, than that calculated to the northwest, it is difficult to place significance on the variability given uncertainties in fault displacements. Recovering D_3 shortening modifies the cross-section in several important ways. Two anticlines, precursors to the Montargull and hanging-wall imbricate thrusts, are reconstructed based on pre-D_3 geometries seen in adjacent sections and a syncline in the Montargull thrust's footwall (Fig. 11b). The fold associated with the Montargull thrust is speculative because its reconstruction included removal of a diapiric overprint inferred to be either a D_3 structure, or younger, similar to other Triassic-cored diapirs seen in the Pyrenees (Pueyo *et al.*, 1991).

Nearly every structure was affected by D_2 deformation (Fig. 11b & c). The only unaffected structure is a north-vergent thrust near the leading edge of the Sierras Marginales thrust sheet (Fig. 12a). One of the most spectacular D_2 structures is a large displacement thrust ($\sim$2 km) on which a panel of folded pre-tectonic strata were displaced over unit 1 (Figs 11 & 12a). In some cases, partial restoration of D_2 shortening on faults results in the reconstruction of folds. This interpretation is justified by incomplete back rotation of footwall synclinal limbs following unfolding of unit 1 and unconformities beneath Middle Eocene strata projected onto the line of section from the Ivars section (Fig. 12). Rotation of the hanging-wall units back down the leading edge of Sierras Marginales thrust sheet restores the offset of unit 1 across this fault (Fig. 12b & c). These D_2 structures accommodated 3.5 km of shortening at a rate of 1.7 mm y^{-1}. A relatively simple cross-section comprising two anticlines and two thrust faults is revealed by the removal of D_2 effects (Fig. 11c).

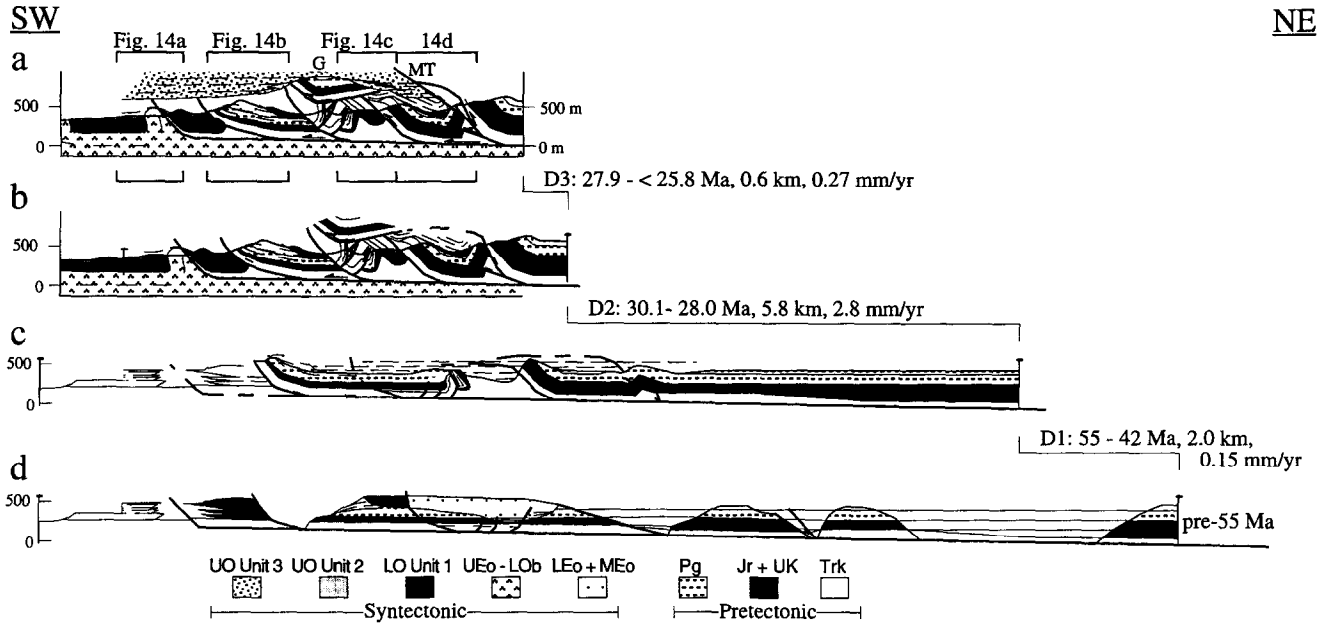

Fig. 13. Sequential restoration for the Ivars section. Each deformational pulse, 1 through 3, is denoted by D_1, D_2, or D_3 and is followed by the age range, amount of shortening in kilometers (km), and shortening rate in millimeters per year (mm yr^{-1} = km my^{-1}). (a) Present, post-D_3 cross-section. (b) Pre-D_3, post-D_2 cross-section. (c) Pre-D_2, post-D_1 cross-section. (d) Fully restored, pre-D_1 cross-section. Age span of D_1 given by biostratigraphic data (Pocoví, 1978). Units are the same as Fig. 3. MT is the Montargull thrust. G is the Gastapá thrust sheet. The positions of the detailed sections in Fig. 15 are indicated by open boxes. See Fig. 3 for location.

Restoration of the three folds and the north-vergent thrust adds an additional 1.5 km to the total shortening (Fig. 11d). A relatively low shortening rate, 0.12 mm y^{-1} is indicated for D_1 deformation. This rate is approximately the same as that of D_1 deformation on the Baldellou section.

Ivars—structural geometries

Structure adjacent to the Ivars section is remarkably complex. Like the other sections, D_1 deformation is marked by angular unconformable relationships between pre-tectonic and Eocene limestones and unit 1 strata (Fig.

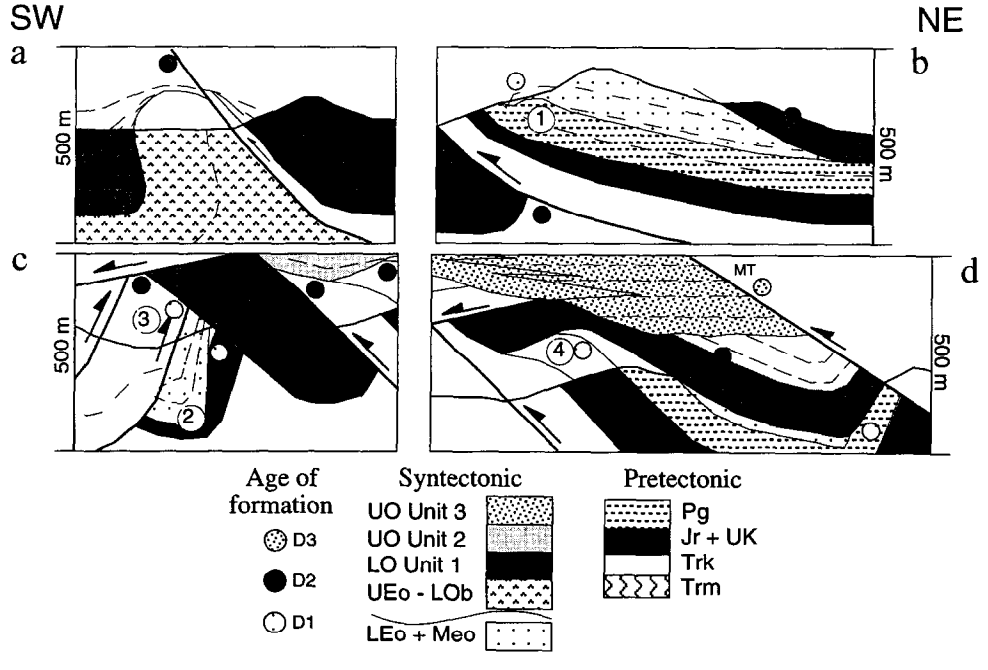

Fig. 14. Details of the Ivars section. D_1, D_2, and D_3 refer to structures and tilts formed during deformational pulses 1, 2, and 3, respectively. Stratigraphic and/or structural evidence for a particular deformational pulse are denoted by shaded dots. MT is the Montargull thrust. Units as in Fig. 3. Circled numbers are points on sections referred to specifically in the text.

14). Unlike the other sections, the limestones are Middle, rather than Early, Eocene in age (Pocoví, 1978). Complex geometrical relationships are seen across these unconformities. For example, anticlinally-folded Middle Eocene rocks overlie homoclinally north-dipping pre-tectonic strata in one thrust sheet (1, Fig. 14b). An angular unconformable contact between Middle Eocene and underlying pre-tectonic strata is inferred (Fig. 14b). One implication of this interpretation is that folding of Middle Eocene strata may have resulted from differential layer-parallel slip within the pre-tectonic strata (Alonso, 1989).

In a single outcrop in the footwall Gastapá thrust sheet, a very complex structure provides additional evidence of D_1 deformation on the Ivars section (Figs 3 & 14c). Pre-tectonic rocks are truncated below an unconformity at the base of a conglomerate (2, Fig. 14c). The conglomerate is inferred to be Middle Eocene in age because it unconformably overlies Lower Eocene rocks and is unconformably overlain by unit 1. Beds within the Middle Eocene (?) conglomerate onlap the unconformity and dip less steeply to the south than underlying pre-tectonic strata. These conglomerates are cut by a north-vergent thrust (3, Fig. 14c). The fault, conglomeratic strata and basal unconformity and pre-tectonic strata are all unconformably overlain by unit 1. Contact relationships between unit 1 and an anticline–syncline pair in the hanging-wall of the next thrust sheet to the northeast indicate the fold pair initially formed during D_1 deformation (4, Fig. 14d). The unconformity at the base of unit 1 truncates the crest of the anticline and beds within unit 1 onlap the limbs of the folds and dip less steeply than pre-tectonic strata (Figs 3 & 8d). Clearly some folding occurred during D_1 prior to the deposition of unit 1.

Each exposure of unit 1 on the Ivars is truncated on the northeast by a south-vergent thrust (Fig. 3). Growth strata are seen in unit 1 on both limbs of the southwestern most fold on the Ivars section (Fig. 14a). The fold is interesting in that its southern limb consists of the Barbastro Formation overlain by unit 1, but its northern limb includes the Sierras Marginales thrust, Triassic evaporites and unit 1. This suggests that the Sierras Marginales thrust sheet was emplaced prior to unit 1 deposition but after Barbastro Formation deposition. Folding of unit 1 was post-emplacement and superimposed on pre-existing structures. Unit 1 on the north limb is cut by the next thrust to the northeast, which in addition to carrying folded Middle Eocene strata, carries folded unit 1 strata (Fig. 14b). Unit 1 probably onlaps the Middle Eocene rocks given that it was deposited in a pre-existing structural low.

Unit 1 is also folded into a syncline in its next exposure to the northeast (Fig. 14c). It is inferred to onlap the unconformity on the southwest limb of the syncline. In the next thrust sheet to the northeast, unit 1 unconformably overlies and is folded about an underlying anticline–syncline pair seen in pre-tectonic strata. Reactivation of a fold initially formed during D_1 is indicated by these observations (Fig. 14d). The Montargull thrust cuts the northeast limb of the syncline. Unit 1 in this thrust sheet and the one immediately to the southwest lie structurally below and are truncated beneath the Gastapá thrust sheet (Fig. 3) interpreted to be a klippe of a thrust sheet displaced over underlying structures. Because the klippe lies on unit 1 locally and is unconformably overlain by unit 3 (Figs 3 & 14d), its emplacement must have occurred during D_2. With the exception of the Montargull thrust, each fault and fold affecting unit 1 is either unconformably overlain by unit 3 or is cut by a fault overlain by unit 3 (Fig. 3).

The only evidence for D_3 deformation on the Ivars section is the Montargull thrust which cuts unit 3 (Figs 3 & 14d). It is difficult to determine whether Unit 3 is gently folded as it is on the Baldellou section because it is dominated by poorly exposed evaporites. In contrast, conglomeratic bodies, interpreted as alluvial fans emanating from adjacent structural highs, are well exposed and interfinger with the lacustrine facies (Fig. 14d).

Ivars—sequential restoration and incremental displacement field

Despite the fact that the structural complexity of the Ivars section exceeds both the Ribagorzana and Baldellou sections, the sequence of deformation and overprinting is equally well-constrained (Fig. 13). Shortening during D_3 is modest, in comparison with that during D_2 and D_1 and consists of a 0.6 km displacement on the Montargull thrust. It seems likely that unit 3 is folded, but folds could not be identified in the field. A D_3 shortening-rate of 0.27 mm y^{-1}, similar to that on the Baldellou section, is given for the Ivars section. An anticline is partially restored when the Montargull thrust displacement is removed, although the anticline is not completely reconstructed because a splay from the lower thrust is not restored (Fig. 13b).

Major deformation in the Ivars section, as in the other two sections, occurred during D_2 deformation. Every exposure of unit 1 is synclinally folded as a consequence of fold reactivation, fault reactivation by renewed translation up a thrust ramp, or hanging-wall back rotation by footwall deformation (Figs 13b & 14). Restoring these tilts involves removing both fault displacement and folding (Fig. 13c). The most significant D_2 event is the emplacement of the Gastapá thrust sheet over folded unit 1 and other previously formed structures (Fig. 13b). The map pattern of the Gastapá thrust sheet demands that it root to the northeast in the Montargull thrust zone (Fig. 3). A systematic increase in D_2 shortening (5.8 km on the Ivars section), rate of shortening (2.8 mm y^{-1} for the Ivars section) and structural complexity is seen between neighboring sections from northwest to southeast, respectively. Two south-vergent thrusts, one north-vergent thrust and two folds remain in the section after D_2 structure is retro-

deformed (Fig. 13c). Note that the southwesternmost thrust and the north-vergent thrust and its footwall syncline all steepen as a consequence of the removal of D_2 structure.

A final 2.0 km of shortening is recovered when the remaining structures are restored (Fig. 13d). This restoration implies a shortening rate of 0.15 mm y^{-1}, larger than both the Baldellou and Ribagorzana sections. In addition to being constrained by unfolding unit 1, D_1 is recorded by tilt below Middle Eocene rocks (Fig. 14b & c), rather than Lower Eocene limestones as seen on both the Baldellou and Ribagorzana sections (Figs 10c & 12). Because this section is less deeply eroded, several consequences of the full restoration for stratigraphy can be highlighted. Whereas Lower Eocene limestones always lie conformably over Paleocene rocks, Middle Eocene rocks, in contrast, overlie a variety of pre-tectonic units, commonly above angular unconformities. Mesozoic stratigraphic thicknesses are variable in the southern portions of the restored stratigraphic wedge. In particular, the greatest variability in thickness and preservation of Mesozoic strata is seen in the Ivars section.

DISCUSSION

The bracketing of deformational ages with syntectonic deposits is one source of uncertainty. Consideration of D_1 deformation highlights the potential uncertainty. D_1 spans 13 my and is marked by growth strata in Lower Eocene limestones, growth strata and unconformities beneath Middle Eocene strata and angular unconformable relationships beneath unit 1. Nearly every structure on each of the three sections is unconformably overlain by unit 1 (Figs 9a, 11a & 13a). Lower Eocene growth strata are preserved on one structure per section on the Ribagorzana and Baldellou sections, respectively. Middle Eocene rocks are preserved on only two structures on the Ivars section, in contrast. Given that Middle Eocene deformation can be discriminated from Early Eocene deformation elsewhere in the south-central Pyrenees (Pocoví, 1978; Mutti *et al.*, 1985; Martínez *et al.*, 1988; Muñoz, 1992; Puigdefàbregas *et al.*, 1992; Vergés, 1993), D_1 structures likely formed during two or more discrete deformational pulses. Whereas evidence of folding and faulting is abundantly preserved below unit 1, discrete Middle and Early Eocene periods of folding and thrusting cannot be isolated. These observations justify differentiation of D_1 structures from D_2 or D_3 structures, even though the duration of deformation, degree of folding and faulting and rates of shortening attributed to D_1 may, in fact, be the product of more than one deformational pulse.

Nearly every structure formed during D_1 deformation was active again during D_2 time (Figs 9, 11 & 13). Distributed and complex temporal patterns of thrusting have been revealed where high-resolution age control, like that in the study area, is available (some examples include: western Himalaya—Burbank and Raynolds, 1988; Moroccan Rif—Morley, 1992; Idaho–Wyoming–Utah—Wiltschko and Dorr, 1983; Coogan, 1992; DeCelles *et al.*, 1993; DeCelles, 1994; DeCelles and Mitra, 1995). Although such age control offers an unique view of the temporal distribution of deformation, the fact that there is a limit to its resolution requires that thrust sequence, at some temporal level, cannot be resolved. Few structural or stratigraphic observations provide insight into the structural sequence during either D_1 or D_2, for example. It is not possible to say with confidence how one D_2 structure moved relative to any other D_2 structures. The absolute temporal resolution limits the extent to which the kinematic history can be resolved.

Restoration of fault displacement during any of the three deformational episodes gives only a minimum value when the hanging-wall cutoff is eroded (Woodward *et al.*, 1985). Furthermore, an individual chron on the geomagnetic polarity time scale represents the shortest interval of time resolvable by magnetostratigraphy (Talling and Burbank, 1993). The differences between D_3 shortening (and rates) on the Ivars and Baldellou sections and the Ribagorzana section (0.6 km versus 1.2 km) arises primarily from uncertainty in restoring fault slip. Even though the sections are geometrically viable because they are restorable (Elliott, 1983), they may still not be 'correct' because of uncertainties in the absolute displacement of individual faults and the sub-chron-scale temporal partitioning of slip accumulation (Geiser, 1988).

In contrast to the uncertainties cited above, the difference between the D_2 shortening and rates calculated for the Baldellou, Ribagorzana and Ivars sections is geologically significant (Figs 9, 11 & 13, respectively). Two important questions are raised: (1) what are the implications of large, along strike differences in shortening within a thrust sheet and (2) what factors contributed to the differences in structural geometry along strike from northwest to southeast? Substantial differences in shortening along strike require the formation of transform-like tear faults or vertical axis rotations. A few tear faults were mapped with an appropriate sense of offset (Fig. 3), but they are too few and have too little displacement to accommodate the differences in offset. Therefore a 25° clockwise vertical axis rotation of the Ivars sections with respect to the Baldellou section is required with an angular velocity of $\sim 12°$ my^{-1} The paleomagnetic data are probably not substantially affected by this rotation because they were collected adjacent to the Baldellou section.

The rotation was probably accommodated by a few faults. For example, emplacement of Gastapá thrust sheet on the Ivars section (~ 4 km, Fig. 13b) probably accounts for a substantial proportion of the rotation. Likewise, the large D_2 overthrust on the Ribagorzana section is pinned by the unconformity at the base of unit 1 to the northwest (point C, Fig. 3), but it overthrusts unit 1 by as much as 2 km to the southeast (Fig. 11b). On this

fault, the map relationships suggest that the northwestern-portion of the fault remained pinned despite the fact that displacement increased to the southeast. It is inferred, therefore, the D_2 displacement was not accompanied by tip propagation but by vertical-axis rotation. A more complicated length–displacement relationship than that implied for many faults is implied (Elliott, 1976; Walsh and Watterson, 1988).

Fold reconstruction at the present-day sites of thrust faults is a by-product of the sequential restorations. The widespread occurrence of footwall synclines, a few hanging-wall anticlines and growth sequences in the core of many of the synclines all support the interpretation that many of the faults were localized at sites of earlier folding (Ramsay, 1992; McNaught and Mitra, 1993). One possible interpretation of this outcome is that the folds and faults grew contemporaneously as fault-propagation folds that, subsequently, were truncated by breakthrough of the fault across the anticlinal forelimb (Mitra, 1990; Suppe and Medwedeff, 1990). Initial buckling and detachment folding followed by thrust truncation represents an alternative kinematic history (Cooper and Trayner, 1986; DeCelles *et al.*, 1991; Fischer and Woodward, 1992; Fischer *et al.*, 1992; Vergés *et al.*, 1996). In fact, the later interpretation is preferred for the following reasons (Fig. 15): (1) footwall synclines are common and suggest that folding pre-dates faulting (Ramsay, 1992; McNaught and Mitra, 1993); (2) in many of the folds, limb angles decrease during sequential restoration; (3) dips in growth strata sequences systematically decrease from steeper to shallower with decreasing structural and stratigraphic position (DeCelles *et al.*, 1991; Vergés *et al.*, 1996); (4) fault trajectories in the deformed state are smooth and less-steeply dipping than in the restored state, which suggests that the faults cut previously folded strata (Cooper and Trayner, 1986).

The 'fold-first' interpretation for many of the structures is note-worthy (Fig. 15). In the absence of a footwall syncline, the footwalls of thrusts in the subsurface are often interpreted as undeformed like that expected in a fault-first structure (a fault-bend fold geometry, for example). A range of kinematic interpretations for fold–fault relationships are permissible, particularly in the presence of footwall folding. Commonly, footwall interpretations default to an undeformed geometry, when data to the contrary are absent, without regard for the kinematic implications (Woodward *et al.*, 1985). Such an interpretation was adopted for several structures in this study because it was geometrically simple and honored the available data with the least bias. The many structures associated with well-preserved evidence of late-stage faulting following intermediate-stage folding suggests interpretations in which footwall geometries are inferred to be synclines are equally valid.

The extent of deformation, in terms of numbers of structures and structural complexity, adjacent to the Rio Ribagorzana is impressive. Stratigraphy may have influenced the style deformation. The pre-tectonic strata are thin on the southwestern edge of the Sierras Marginales thrust sheet (< 300 m thick). In particular, the Jurassic through Paleocene package displays substantial variability in thickness and stacking. When the total restorations of the Baldellou and Ivars sections are compared, a connection between stratigraphic variability and structural style is suggested (Fig. 13). A simple imbricate fan thrust system is associated with a gradually northward-thickening stratigraphic wedge along the Baldellou section (Fig. 9). Large-scale overthrusting and north- and south-vergent thrusting are associated with a

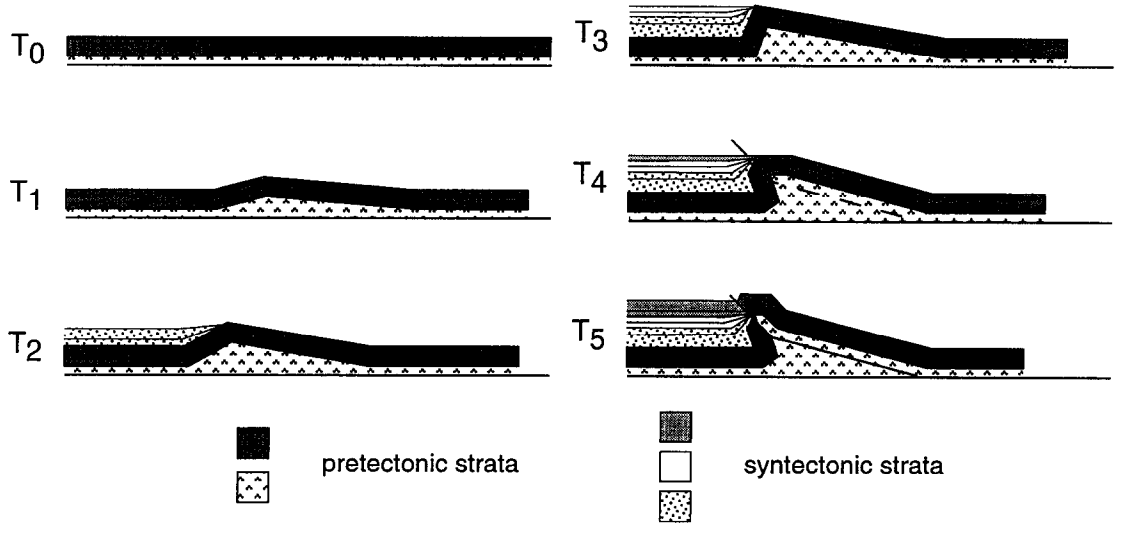

Fig. 15. Schematic forward-model depicting the relationship between folding and thrust faulting. Note that thrust fault formation and displacement takes place after a substantial amount of rotating-limb detachment folding. Exact geometric relationships within the fold are diagrammatic. Syntectonic strata (3 units) has been included to illustrate its role in delineating structural geometry and the relationship between folding and faulting with time. The symbol T_x denotes non-scaled time increments.

highly variable stratigraphic sequence on the Ivars section (Fig. 13). It is concluded that stratigraphic variability played a significant role in both the style and evolution of major structures.

Units 1 and 3 have stratigraphically and structurally correlative units 25 km to the west at Peralta de la Sal and 40 km to the east at Artesa de Segre that allow this study to be cast in a regional framework (Fig. 2). Unit 1 (30.1–28.5 Ma), which is characterized by locally-derived detritus, deposition on top of the Sierras Marginales thrust sheet and extensive deformation, correlates with the Peraltilla Formation at Peralta de la Sal (Senz and Zamorano, 1992) and with informal unit 2 (29.5–28.5 Ma) at Artesa de Segre (Meigs *et al.*, 1996). Unit 3 (27.9–<25.8 Ma), which is characterized by a hinterland provenance and only local deformation, correlates with the Sariñena Formation at Peralta de la Sal and with informal unit 3 (27.8–<24.7 Ma) at Artesa de Segre. Extrapolation of the ages of units 1–3 to Peralta allows temporal correlation of the structural histories across the width of the south-central unit of the Pyrenees (Fig. 2).

The oldest event common to the three areas is translation of the Sierras Marginales thrust sheet over previously-folded foreland basin deposits. In the study area, translation of the Sierras Marginales thrust sheet is inferred to have occurred before ~30 Ma, between deposition of the Barbastro Formation (top is Lower Oligocene, ~33 Ma) and unit 1 (30.1 Ma) because the thrust sheet is interpreted to sit on the Barbastro Formation and unit 1 was deposited above the Barbastro Formation, the hanging-wall and footwall of the thrust sheet (Figs 9a, 11a & 13a). The Peraltilla Formation also overlies the hanging-wall of the Sierras Marginales thrust sheet and previously-folded foreland deposits in the footwall (Senz and Zamorano, 1992). Translation of the Sierras Marginales thrust sheet over the foreland basin at Artesa is tightly constrained to have occurred between 32.0 and 29.5 Ma, after initial deformation of the foreland (Meigs *et al.*, 1996). Internal deformation of the Sierras Marginales thrust sheet at Peralta was coeval with deposition of the Peraltilla Formation and the lower part of the Sariñena Formation and occurred between 29.5 and 27.8 Ma at Artesa. These compare well with the internal deformation (D_2: 30.1–28.0 Ma) in the study area. The upper part of the Sariñena Formation unconformably overlies these internal structures but is cut by the Montargull thrust. Formation of the Montargull thrust occurred after 24.7 Ma at Artesa de Segre.

The consistency in the ages of events along the strike length of the front of the south-central unit suggests that the entire front of the Sierras Marginales thrust sheet advanced coevally along strike and reached its present position by ~30 Ma. Internal deformation, in a general sense, was also coeval along strike and occurred between 30 and 28 Ma. In detail, individual structures formed during this period of internal deformation likely developed diachronously along strike. The exception to this generalization, within the resolution of the data, is the Montargull thrust whose displacement everywhere occurred after 26 Ma. Similarities between syntectonic deposits and structural histories at Artesa, Peralta and in this study reveal comparable and internally consistent chronologies of deformation. The absolute ages compare well in time because of the specific magnetic correlation chosen for the paleomagnetic section.

Non-marine clastic sequences like unit 1 deposited in piggyback basins are widely preserved throughout the Pyrenees. Magneto-stratigraphic chronologies demonstrate that these sequences usually accumulate diachronously. In the study area, strata deposited directly over pre-tectonic strata in the Sierras Marginales thrust sheet range in age from 30.1 to 28.5 my. At Artesa de Segre to the east, rocks in a similar structural and stratigraphic position range in age from 29.5 to 28.5 my and at Oliana, even farther to the east, they range in age from 36.5 to 34.5 my (Fig. 2; Burbank *et al.*, 1992b; Meigs *et al.*, 1996). The diachronous nature of these non-marine rocks limits the confidence with which biostratigraphic data may be extrapolated from one basin to another. Moreover, the sequential restorations, although they reflect the products of deformational events that occurred coevally in space and time in general, likely depict geometries and structures that evolved diachronously within a deformational period, in detail. These basin-margin structures control deposition in associated piggyback basins; basin fill is expected to have fill-ages that are more directly coupled with local patterns of deformation than with regional controls on sedimentation (Coogan, 1992). High sediment accumulation rates in unit 1 and its structural and stratigraphic equivalent at Artesa de Segre attest to initially rapid infilling on formation (Fig. 8c) (Meigs *et al.*, 1996). Sediment-accumulation rates decelerate after basins become filled, local relief is over-topped by sediment and regionally established drainage systems are re-established.

High variability in sediment-accumulation rates reflect the impact of local structure on regional distributary systems. Up to several hundred meters of relief on the basin margins are indicated by the partial restorations (Fig. 13). Although small alluvial fans shed from basin-margin topographic highs indicate that basin margins are continually eroding, the fact that the topography is created by uplift of relatively resistant carbonate material suggests that the uplift rate exceeds the rate of erosion. Topography is both created and regenerated as a consequence of formation and reactivation of structures and is maintained as positive relief over the time scale of the total deformation. The highest rates of sediment accumulation are recorded in ponded zones within synclines. Basin margins are marked by onlap, offlap and non-deposition. In contrast, the lowest sediment-accumulation rates correspond with times when more regionally consistent patterns of deposition prevail and

stratal ages, as a consequence, may be less diachronous. Clearly, basin-margin deformation partitions basins and distributary systems only when locally created topography is maintained; when synorogenic topography is reduced by erosion or buried by sediment, regionally controlled variables, which act on longer time scales, control sediment-accumulation rates and dispersal patterns.

CONCLUSIONS

This study demonstrates the utility of syn-orogenic sediments in the discrimination of spatial, temporal and geometrical patterns of deformation.

(1) Three new informal stratigraphic units were recognized in the non-marine stratigraphic succession. Correlation of a new magneto-stratigraphic section with the geomagnetic polarity time scale (Cande and Kent, 1992) provides age control for the three units: unit 1 is 30.1 to 28.5 my old, unit 2 is 27.9 to 27.0 my old and unit 3 is 27.0 to <25.8 my old.

(2) Four syntectonic units, the three new units in the non-marine rocks and a previously recognized sequence of Lower and Middle Eocene marine limestones, provide evidence for a three-stage deformational history of internal deformation of the Sierras Marginales thrust sheet.

(3) D_1 is a Early to Middle Eocene deformation marked by growth strata in Lower Eocene limestones, angular unconformities beneath Middle Eocene strata and tilted beds below unit 1. Shortening during D_1 ranged from 1.0 to 2.0 km and occurred at rates which varied from 0.08 to 0.15 mm y^{-1}.

(4) D_2 is marked by folding of unit 1 and angular unconformities beneath units 2 and 3. Shortening and rates of shortening varied along strike from northwest to southeast from 1.5 km at 0.7 mm y^{-1} to 5.8 km at 2.8 mm y^{-1}, respectively. This differential shortening implies a 25° clockwise rotation of the southeastern part of the study area with respect to the northwest. The rotation was accommodated to a large extent by two different thrusts, each with greater than 2 km of displacement.

(5) D_3 consists of a bulk tightening and thickening of the hanging-wall of the Sierras Marginales thrust sheet and the formation of the Montargull thrust. Coeval displacement on the Montargull thrust can be seen at least 20 km to the northwest and 40 km to the east-northeast. D_3 shortening was between 0.5 and 1.2 km yielding rates which varied from 0.24 to 0.57 mm y^{-1}.

(6) Nearly every structure was active during D_1 and D_2. There is no clear thrust sequence during any discrete deformational pulse. Distributed deformation by synchronous formation and reactivation of earlier-formed structures dominated the thrust sequence throughout the deformation. Overall, rates of deformation were highly variable with the highest rate of deformation occurring during D_2. This suggests that the deformation was discontinuous in time.

(7) Many thrusts restore, in intermediate sequential reconstructions, to folds. This suggests that the area was characterized by a fold-first structural style. The evolution of a single structure is envisioned to begin by nucleation of a detachment-like fold, rotation of fold limbs to steeper angles and concurrent shortening of the wavelength, leading to formation of a new thrust that cuts the steepened forelimb of the earlier-formed fold.

(8) Young, non-marine alluvial, fluvial and lacustrine rocks preserved throughout the Spanish Pyrenees are diachronous and their ages are a function of the age of formation of local structures. Basin formation, or formation of accommodation space, has greater dependence on the formation of structural barriers than on regional controls on sedimentation. Once formed, these basins experience a period of rapid sediment accumulation perhaps because regional controls on sedimentation are superseded by local controls due to partitioning of depositional and dispersal patterns. Burial of structures by younger deposits is accompanied by a deceleration in sediment-accumulation rates suggesting a return to regional controls on deposition and dispersal patterns.

(9) The structural chronology developed for the leading edge of the Sierras Marginales thrust sheet in the study area compares well regionally. From Artesa de Segre (Meigs *et al.*, 1996) on the east, to the Ribagorzana River region (this study), to Peralta de la Sal on the west (Senz and Zamorano, 1992), final emplacement of the thrust sheet was completed by 30 Ma, internal deformation occurred between 30 and 28 Ma and post-dates the final emplacement and the Montargull thrust, the youngest structure, formed after 26 Ma.

Acknowledgements—This study was conducted as part of a Ph.D. Dissertation under the supervision of Doug Burbank. Doug provided unlimited enthusiasm, insight and feedback and contributed substantially to this work. Josep Anton Muñoz introduced me to the area, spent many days in the field and office discussing all aspects of the study and encouraged me to differentiate syntectonic units. Julio Friedmann and Audrey Huerta are thanked for field assistance. Jaume Vergés and Antonio Teixell are thanked for discussion of Pyrenean geology. Jim Holl, David Anastasio and an anonymous reviewer gave excellent formal reviews of the manuscript for the Journal and are thanked. Dave Anastasio, Eric Erslev and Don Fisher are thanked for their editorial work to produce this special volume. Support for this study was provided by NSF grant EAR-9304863, Donors of the Petroleum Research Fund, Geological Society of America, Sigma Xi, the American Association of Petroleum Geologists and a Shell Foundation Fellowship.

REFERENCES

Alonso, J. L. (1989) Fold reactivation involving angular unconformities: theoretical analysis and natural examples from the Cantabrian Zone (Northwest Spain). *Tectonophysics* **170**, 57–77.

Armstrong, F. C. and Oriel, S. S. (1965) Tectonic development of Idaho–Wyoming thrust belt. *Bulletin of the American Association of Petroleum Geologists* **49**, 1847–1866.

Anadón, P., Cabrera, L., Colombo, F., Marzo, M. and Riba, O. (1986) Syntectonic intraformational unconformities in alluvial fan deposits, eastern Ebro Basin margins (NE Spain). In *Foreland Basins*, eds A.

Allen and Homewood, Vol. 8, pp. 259–271. International Association of Sedimentologists, Special Publication.

Boyer, S. E. (1992) Geometric evidence for synchronous thrusting in the southern Alberta and northwest Montana thrust belts. In *Thrust Tectonics*, ed. K. R. McClay, pp. 377–390. Chapman and Hall, London.

Burbank, D. W. and Raynolds, R. G. H. (1988) Stratigraphic keys to the timing of thrusting in terrestrial foreland basins: Applications to the Northwestern Himalaya. In *New Perspectives in Basin Analysis*, eds K. L. Kleinspehn and C. Paola, pp. 331–351. Springer-Verlag, New York.

Burbank, D. W., Puigdefàbregas, C. and Muñoz, J. A. (1992a) The chronology of Eocene tectonics and stratigraphic development of the eastern Pyrenean foreland basin, northeast Spain. *Geological Society of America Bulletin* **104**, 1101–1120.

Burbank, D. W., Vergés, J., Muñoz, J. A. and Bentham, (1992b) Coeval hindward- and foreward-imbricating thrusting in the south-central Pyrenees, Spain: Timing and rates of shortening and deposition. *Geological Society of America Bulletin* **104**, 3–17.

Butler, R. W. (1992) *Paleomagnetism: Magnetic Domains to Geologic Terranes*. Blackwell Scientific Publications, Boston.

Cande, S. C. and Kent, D. V. (1992) A new geomagnetic polarity time scale for the Late Cretaceous and Cenozoic. *Journal of Geophysical Research* **97**, 13917–13951.

Coogan, J. C. (1992) Structural evolution of piggyback basins in the Wyoming–Idaho–Utah thrust belt. In *Regional Geology of Eastern Idaho and Western Wyoming*, eds K. Link, M. A. Kuntz and L. B. Platt, pp. 55–81. Geological Society of America Memoir.

Cooper, M. A. and Trayner, M. (1986) Thrust-surface geometry: implications for thrust-belt evolution and section-balancing techniques. *Journal of Structural Geology* **8**, 305–312.

Crusafont, M., Riba, O. and Villena, J. (1966) Nota preliminar sobre un nuevo yacimiento de vertebratos Aquitanienses en Sta. Cilia (rio Formiga; Provincia de Huesca) y sus consequencias geologicas. *Notas y Communicaciones IGME* **83**, 7–13.

DeCelles, P. G. (1994) Cretaceous–Paleocene synorogenic sedimentation and kinematic history of the Sevier thrust belt, northeast Utah and southwest Wyoming. *Geological Society of America Bulletin* **106**, 32–56.

DeCelles, P. G., Gray, M. B., Ridgway, K. D., Cole, R. B., Srivastava, P., Pequera, N. and Pivnik, D. A. (1991) Kinematic history of a foreland uplift from Paleocene synorogenic conglomerate, Beartooth Range, Wyoming and Montana. *Bulletin of the Geological Society of America* **103**, 1458–1475.

DeCelles, P. G. and Mitra, G. (1995) History of the Sevier orogenic wedge in terms of critical taper models, northeastern Utah and southwestern Wyoming. *Geological Society of America Bulletin* **107**, 454–462.

DeCelles, P. G., Pile, H. T. and Coogan, J. C. (1993) Kinematic history of the Meade thrust based on provenance of the Bechler conglomerate at Red Mountain, Idaho, Sevier thrust belt. *Tectonics* **12**, 1436–1450.

Elliott, D. (1976) The motion of thrust sheets. *Journal of Geophysical Research* **81**, 949–963.

Elliott, D. (1983) The construction of balanced cross-sections. *Journal of Structural Geology* **2**, 101.

Fischer, M. P. and Woodward, N. B. (1992) The geometric evolution of foreland thrust systems. In *Thrust Tectonics*, ed. K. R. McClay, pp. 181–191. Chapman and Hall, London.

Fischer, M. P., Woodward, N. B. and Mitchell, M. M. (1992) The kinematics of break-thrust folds. *Journal of Structural Geology* **14**, 451–460.

Fisher, R. A. (1953) Dispersion on a sphere. *Proceedings of the Royal Society* **A217**, 295–305.

Geiser, A. (1988) The role of kinematics in the construction and analysis of geological cross sections in deformed terranes. In *Geometries and Mechanisms of Thrusting with Special Reference to the Appalachians*, eds G. Mitra, G. and S. Wojtal, 222, pp. 47–76. Geological Society of America Special Paper.

Jordan, T. E., Flemings, B. and Beers, J. A. (1988) Dating thrust-fault activity by use of foreland-basin strata. In *New Perspectives in Basin Analysis*, eds K. L. Kleinspehn and C. Paola, pp. 307–330. Springer-Verlag, New York.

Marshak, S. and Mitra, G. (1988) *Basic Methods of Structural Geology*. Prentice-Hall, Englewood Cliffs.

Martínez, A., Vergés, J. and Muñoz, J. A. (1988) Sequencias de propagación del sistema de cabalgamientos de la terminación del manto del Pedraforca y relación con los conglomerados sinorogénicos. *Acta Geológica Hispánica* **23**, 119–128.

Martínez-Peña, M. B. and Pocoví, A. (1988) El amortiguamiento frontal de la estructura de la cobertera surpirenaica y su relación con el anticlinal Barbastro-Balaguer. *Acta Geológica Hispánica* **23**, 81–94.

McFadden, P. L. and McElhinny, M. W. (1990) Classification of the reversal test in paleomagnetism. *Geophysical Journal International* **103**, 725–729.

Medwedeff, D. A. (1989) Growth fault-bend folding at southeast Lost Hills, San Joaquin Valley, California. *Bulletin of the American Association of Petroleum Geologists* **73**, 54–67.

McNaught, M. A. and Mitra, G. (1993) A kinematic model for the formation of footwall synclines. *Journal of Structural Geology* **15**, 805–808.

Meigs, A. J., Burbank, D. W. and Muñoz, J. A. (1992) Thrust sequence within the western Sierras Marginales thrust sheet, south-central Pyrenees, Spain. *EOS Transactions of the American Geophysical Union* **73**, 545.

Meigs, A. J., Vergés, J. and Burbank, D. W. (1996) Ten-million-year history of a thrust sheet. *Bulletin of the Geological Society of America* **108**, 1608–1625.

Mitra, S. (1990) Fault-propagation folds: Geometry, kinematic evolution and hydrocarbon traps. *Bulletin of the American Association of Petroleum Geologists* **74**, 921–945.

Morley, C. K. (1988) Out-of-sequence thrusts. *Tectonics* **7**, 539–561.

Morley, C. K. (1992) Tectonic and sedimentary evidence for synchronous and out-of-sequence thrusting, Larache–Acilah area, Western Moroccan Rift. *Journal of the Geological Society, London* **149**, 39–49.

Muñoz, J. A. (1992) Evolution of a continental collision belt: ECORS-Pyrenees crustal balanced section. In *Thrust Tectonics*, ed. K. R. McClay, pp. 235–246. Chapman and Hall, London.

Mutti, E., Rosell, J., Allen, G. P., Fonnesu, F. and Sgavetti, M. (1985) The Eocene Baronia tide dominated delta-shelf system in the Ager Basin. In *IAS 6th Regional Meeting Excursion Guidebook*, eds M. D. Mila and J. Rosell, pp. 579–600. International Association of Sedimentologists.

Pocoví, J. (1978) Estudio geologico de las Sierras Marginales Catalanas (Prepirineo de Lerida). Unpublished Ph.D. thesis, Universitat de Barcelona.

King-Powers, M. M. K. (1989) Magnetostratigraphy and rock magnetism of Eocene foreland basin sediments, Esera and Isabena River valleys, Tremp–Graus basin, southern Pyrenees, Spain. Unpublished M.Sc. thesis, University of Southern California.

Pueyo, J. J., Vergés, J. and Salvany, J. M. (1991) Salt-related structures in northern Spain. Barcelona. *Field Guide University of Barcelona*, 54 pp.

Puigdefàbregas, J., Muñoz, J. A. and Vergés, J. (1992) Thrusting and foreland basin evolution in the Southern Pyrenees. In *Thrust Tectonics*, ed. K. R. McClay, pp. 247–254. Chapman and Hall, London.

Ramsay, J. G. (1992) Some geometric problems of ramp-flat thrust models. In *Thrust Tectonics*, ed. K. R. McClay, pp. 191–200. Chapman and Hall, London.

Ramsay, J. G. and Huber, M. I. (1987) *The Techniques of Modern Structural Geology, Volume 2: Folds and Fractures*. Academic Press, London.

Riba, O. (1976) Syntectonic unconformities of the Alto Cardener, Spanish Pyrenees: A genetic interpretation. *Sedimentary Geology* **15**, 213–233.

Royse, F. J., Warner, M. A. and Reese, D. L. (1975) Thrust belt structural geometry and related stratigraphic problems Wyoming–Idaho–Northern Utah. In *Deep Drilling Frontiers of the Central Rocky Mountains*, ed. D. W. Bolyard, pp. 41–54. Rocky Mountain Association of Geologists, Denver.

Senz, J. G. and Zamorano, M. (1992) Evolución tectónica y sedimentaria durante el Priaboniense superior–Mioceno inferior, en el frente de cabalgamientos de las Sierras Marginales occidentales. *Acta Geológica Hispánica* **27**, 195–209.

Sudre, J., de Bonis, L., Brunet, M., Crochet, J.-Y., Duranthon, F., Godinot, M., Hartenberger, J.-L., Jehenne, Y., Legendre, S., Marandat, B., Remy, J. A., Ringeade, M., Sigé, B. and Vianey-Liand, M. (1992) La biochronologie mammalienne du paléogène au Nord et au Sud des Pyrénées: état de la question. *Comptes Rendus Academie Science Paris* **314**, 631–636.

Suppe, J. and Medwedeff, D. A. (1990) Geometry and kinematics of fault-propagation folding. *Eclogae Geologicae Helveticae* **83**, 409–454.

Suppe, J. S., Chou, G. T. and Hook, S. C. (1992) Rates of folding and faulting determined from growth strata. In *Thrust Tectonics*, ed. K. R. McClay, pp. 105–122. Chapman and Hall, London.

Talling, J. and Burbank, D. W. (1993) Assessment of uncertainties in magnetostratigraphic dating of sedimentary strata. In *Applications of Paleomagnetism to Sedimentary Geology*, eds D. J. Aïssaoui, D. F. McNeil and N. F. Hurley, Vol. 49, pp. 59–69. Society of Economic Paleontology and Mineralogy Special Publication.

Teixell, A. (1992) Estructura alpina en la transversal de la terminación occidental de la Zona Axial Pirenaica. Unpublished Ph.D. thesis, Universitat de Barcelona.

Vergés, J. (1993) Estudi Tectònic del Vessant Sud del Pirineu Oriental i Central: Evolució Cinemàtica en 3D. Unpublished Ph.D. thesis, Universitat de Barcelona.

Vergés, J., Burbank, D. W. and Meigs, A. J. (1996) Unfolding: An inverse approach to fold kinematics. *Geology* **24**, 175–178.

Walsh, J. J. and Watterson, J. (1988) Analysis of the relationship between displacement and dimensions of faults. *Journal of Structural Geology* **10**, 239–247.

Wiltschko, D. V. and Dorr, J. A. (1983) Timing of deformation in overthrust belt and foreland of Idaho, Wyoming and Utah. *Bulletin of the American Association of Petroleum Geologists* **67**, 1304–1322.

Woodward, N. B., Boyer, S. E. and Suppe, J. (1985) *An Outline of Balanced Cross-sections*. University of Tennessee, Knoxville.